QUANTUM FLUCTUATIONS OF THE ORDER PARAMETER IN SUPERCONDUCTING NANOWIRES

TANELI RANTALA

Master's thesis
University of Jyväskylä
Department of physics
31.12.2013
Supervisor: Konstantin Arutyunov

Acknowledgements

The research done in this thesis has been carried out at the Quantum nanoelectronics group in the University of Jyväskylä. The work was supervised by Docent Konstantin Arutyunov. I also want to thank Mr. Janne Lehtinen who helped me with the measurements and practical problems.

Table of Contents

1 Abstract

Conventional electron-beam lithography and shadow evaporation techniques in ultra high vacuum were used to fabricate high-ohmic Al-AlO_x-Ti SIS-junctions. Quantum fluctuations of the energy gap Δ_{Ti} of titanium nanowires were studied by measuring $R(T)$- and $I(V)$-characteristics of these junctions. Measurements were done in electromagnetically shielded cryostat at base temperature of $T = 26$ mK. Results show that the thinnest wires do not demonstrate pronounced superconducting $R(T)$ transition. QPS phenomenon explains well broadening of the $R(T)$ transition curves. Differential conductance data (obtained along $I(V)$) shows qualitatively the broadening of energy gap Δ_{Ti} as a function of diameter σ of the nanowire. From these results it can be concluded that QF phenomenon is most likely responsible for the broadening of the energy gap. More study is needed to understand the differences between measured samples which all exhibit large difference in their $I(V)$-characteristics and $\Delta(\sigma)$ dependence. Fluctuations of the energy gap and QPS phenomenon are both universal and should happen in all superconductors. Rate of QPS (and thus fluctuations of the gap) can be affected a lot by choosing the correct material, titanium being a convenient one, and that possibility should be explored. In future studies other materials, for example, zirkonium, could be studied.

2 Introduction

Superconductivity was discovered already in 1911 by K. Onnes, but theory of it was not understood in several decades. In 1957 J. Bardeen, L. N. Cooper and J. R. Schieffer developed the microscopic theory, often called BCS-theory, that revolutionized our understanding of superconductivity. Theory introduces two mutually linked parameters related to superconductors: energy gap Δ and critical temperature T_c. Parameter Δ corresponds to the energy required to break a current carrying quasiparticle, a Cooper pair, in a superconductor. It has a complex value $\Delta = |\Delta|e^{i\varphi}$, where $|\Delta|$ is the amplitude and φ is the phase. Critical temperature is a temperature limit above which the superconducting state is destroyed. Both parameters are material dependent and can be said to be constant in a bulk superconductor. However, in a 1-dimensional superconducting nanowire both parameters vary as a function of the diameter of the wire. Variation of Δ is due to quantum fluctuations, also known as Quantum Phase Slips (QPS). This means that there is no longer a single value for Δ, but both the amplitude and the phase have a Gaussian distribution around an expectation value (which again varies as a function of diameter). Thermally activated phase slips (TAPS) can also affect Δ, and to prevent this the measurements are done in ultra low temperatures where QPS is dominant and TAPS is insignificant. Main objective in this thesis is to systematically study the size dependence of the variable $\Delta(T_c,\rho)$ and fluctuations of Δ. An important point here is to understand that there are two kinds of fluctuations of the order parameter: small continuous fluctuations around the expectation value, and 'large' fluctuations, QPS events, that momentarily destroy superconductivity completely. Main interest in this thesis lie in the smaller fluctuations. Research is done by studying $R(T)$- and $I(V)$-characteristics of S_1IS_2-junctions, where SIS stands for 'Superconductor 1 - Insulator - Superconductor 2'. $I(V)$ measurements give direct information about the size dependence and 'smearing' of the energy gap Δ. $R(T)$ on the other hand gives more information how QPS affects the superconducting transition and about the variations of T_c. Main results from $I(V)$ measurements showed that the fluctuations of the energy gap Δ increase as the diameter *rho* is decreased. Variation of the expectation value

of the energy gap as a function of the diameter is minimal. $R(T)$ measurements showed that the superconducting $R(T)$ transition disappears completely in the smallest nanowires, and the diameter has significant relation to critical temperature: smaller the wire, smaller the T_c.

First I will go through the related theory. This part consists of the BCS theory, superconductivity in 1-dimensional nanowires and the concept of phase slips (both thermal and quantum). After that I will explain the measurements in detail: how samples were fabricated and measured, and results analysed. The last chapters are dedicated to the results.

3 Theory

3.1 Superconductivity

3.1.1 BCS theory and the energy gap Δ

In the superconducting state electrons of the material have attractive net potential, and they form so called Cooper pairs which do not scatter inside the superconductor. This leads to zero electrical resistivity inside the superconductor. This is the most well known property of superconductivity but many more do exist. Microscopic theory was developed in 1957 by J. Bardeen, L. N. Cooper and J. R. Schieffer and because of it we today understand many of these phenomena. In this thesis, we are particularly interested in superconducting energy gap Δ and critical temperature T_c. Both Δ and T_c are material dependent parameters, and within the 'orthodox' BCS theory are related as $\Delta(T = 0) = 1.764 k_B T_c$, where k_B is the Boltzmann constant. Next I show how the bound state that arises from the attractive net potential between the electrons leads to a definition of the energy gap Δ.

With the 2nd quantization notes the pairing Hamiltonian takes form (using standard notations)

$$\hat{H} = \sum_{\vec{k}\vec{\sigma}} \epsilon_{\vec{k}} n_{\vec{k}\vec{\sigma}} + \sum_{\vec{k},\vec{l}} V_{\vec{k}\vec{l}} c^{\dagger}_{\vec{k}\uparrow} c^{\dagger}_{-\vec{k}\downarrow} c_{-\vec{l}\downarrow} c_{\vec{l}\uparrow}, \tag{1}$$

where $\vec{k}$ and $\vec{l}$ are wavevectors, $V_{\vec{k}\vec{l}}$ is the interaction potential, $\vec{\sigma}$ is spin and $n_{\vec{k}\vec{\sigma}} = c^{\dagger}_{\vec{k}} c_{\vec{k}}$ is the total particle number on state $\vec{k}$. By including the term $-\mu N_{op}$ where μ is the chemical potential and N_{op} is the particle number operator, it is possible to regulate the mean number of particles. Next step is to minimize expectation value of the energy of the sum as a function of $\vec{k}$ by setting

$$\delta \langle \psi_G | \hat{H} - \mu N_{op} | \psi_G \rangle = 0. \tag{2}$$

Result of this operation takes form

$$\delta \langle \psi_G | \hat{H} - \mu N_{op} | \psi_G \rangle = 2 \sum_{\vec{k}} \xi_{\vec{k}} v^2_{\vec{k}} + \sum_{\vec{k}\vec{l}} V_{\vec{k}\vec{l}} u_{\vec{k}} v_{\vec{k}} u_{\vec{l}} v_{\vec{l}}. \tag{3}$$

Here $|v_{\vec{k}}|^2$ is the probability of the pair $(\vec{k}\uparrow, \vec{k}\downarrow)$ being occupied and $|u_{\vec{k}}|^2$ is the probability of it not being occupied. $\xi = \epsilon_{\vec{k}} - \mu$ is a single particle energy relative to the Fermi energy. It should be noted that the ξ here should not be confused with the coherence length of superconductor, usually also noted by ξ. By setting the condition

$$|u_{\vec{k}}^2| + |v_{\vec{k}}^2| = 1$$

and choosing

$$\begin{aligned} u_{\vec{k}} &= \sin(\theta_{\vec{k}}) \\ v_{\vec{k}} &= \cos(\theta_{\vec{k}}) \end{aligned} \tag{4}$$

it is possible to reform the equation by trigonometric identities. Then differentiating the expectation value with respect to $\theta_{\vec{k}}$ we get

$$\tan(2\theta_{\vec{k}}) = \sum_{\vec{l}} \frac{V_{\vec{k}\vec{l}} \sin(2\theta_{\vec{l}})}{2\xi_{\vec{k}}}. \tag{5}$$

From this form we can now *define* the energy gap to be

$$\Delta_{\vec{k}} = -\sum_{\vec{l}} V_{\vec{k}\vec{l}} u_{\vec{k}} v_{\vec{l}} = \frac{1}{2} \sum_{\vec{l}} V_{\vec{k}\vec{l}} \sin(2\theta_{\vec{l}}) \tag{6}$$

and the excitation energy of a quasi-particle with a momentum $\hbar\vec{k}$

$$E_{\vec{k}} = \sqrt{\Delta_{\vec{k}}^2 + \xi_{\vec{k}}^2}. \tag{7}$$

These definitions lead to

$$\begin{aligned} \tan(2\theta_{\vec{k}}) &= -\frac{\Delta_{\vec{k}}}{\xi_{\vec{k}}} \\ \sin(2\theta_{\vec{k}}) &= \frac{\Delta_{\vec{k}}}{E_{\vec{k}}} \\ \cos(2\theta_{\vec{k}}) &= -\frac{\xi_{\vec{k}}}{E_{\vec{k}}}. \end{aligned} \tag{8}$$

By substituting Eq. (8) into (6) and applying Cooper approximation for $V_{\vec{k}\vec{l}} = V$ we get

$$\Delta_{\vec{k}} = \begin{cases} \Delta & \text{for } |\xi_{\vec{k}}| < \hbar\omega_c \\ 0 & \text{for } |\xi_{\vec{k}}| > \hbar\omega_c \end{cases} \tag{9}$$

where $\hbar\omega_c$ is the cut-off energy. In this approximation Δ is independent of $\vec{k}$. This approximation really justifies the name 'energy gap', as it is now the minimum excitation energy of a quasi-particle. We get a self-consistency equation from Eq. (5)

$$1 = \frac{V}{2} \sum_{\vec{k}} \frac{1}{E_{\vec{k}}}. \tag{10}$$

This can be calculated by changing the summation to an integration from 0 to $\hbar\omega_c$ and using the weak-coupling limit. This results in a simple equation for the gap:

$$\Delta = \frac{\hbar\omega_c}{\sinh(\frac{1}{N(0)V})} \approx 2\hbar\omega_c e^{-\frac{1}{N(0)V}}. \tag{11}$$

It is also possible to compute the two coefficients $u_{\vec{k}}$ and $v_{\vec{k}}$

$$\begin{aligned} v_{\vec{k}}^2 &= \frac{1}{2}\left(1 - \frac{\xi_{\vec{k}}}{E_{\vec{k}}}\right) = \frac{1}{2}\left(1 - \frac{\xi_{\vec{k}}}{\sqrt{\Delta^2 + \xi_{\vec{k}}^2}}\right) \\ u_{\vec{k}}^2 &= \frac{1}{2}\left(1 + \frac{\xi_{\vec{k}}}{E_{\vec{k}}}\right) = 1 - v_{\vec{k}}^2 \end{aligned} \tag{12}$$

It should be kept in mind that this above result does not hold for strongly coupled superconductors where $N(0)V \gg 1$. However, it is not a concern in this thesis because superconductors used in the measurements, aluminum and titanium, are both in weak coupling limit. More detailed derivation of the energy gap Δ can be found in [1].

3.1.2 Ginzburg-Landau Theory

Short overview of the Ginzburg-Landau (GL) theory is required before explaining 1-dimensional superconductivity, as some of the parameters and con-

cepts come straight from the GL theory. The model is very intuitive and it is a powerful tool when dealing with spatially inhomogeneous superconductors. It should be kept in mind that in the derivation of the GL theory it is assumed that the temperature T is close to critical temperature T_c. This leads to the fact that the GL theory does not give good results when going significantly lower temperatures, as is the case in this thesis.

GL theory was developed by V. L. Ginzburg and L. D. Landau [2] in 1950. It can be derived from the BCS theory as a limiting case where temperature T is close to T_c and the wavefunction and vector potential $\vec{A}$ vary sufficiently slowly. It was done by Gor'kov [3] in 1959. The starting point of the GL theory is a pseudowavefunction $\psi(x)$ which is known as a complex order parameter. Then $|\psi(x)|^2$ describes a *local* density of superconducting electrons $n_s(\vec{r})$. In light of this definition it is easy to think that GL theory describes a macroscopic wavefunction of a superconductor. GL theory also introduces another important parameter (a length scale), Ginzburg-Landau coherence length ξ, in which the order parameter $\psi(x)$ is approximately constant. Dimensionality of the supercondcutor is defined by this material dependent value ξ. ξ is defined to be

$$\xi^2 = \frac{\hbar^2}{2m^*|\alpha(T)|} \tag{13}$$

where

$$\alpha = -\frac{2e^2}{mc^2} H_C^2(T)\lambda_{eff}^2(T). \tag{14}$$

Here H_C is the critical magnetic field and λ_{eff} an effective London penetration depth. H_C is a value of the magnetic field which is powerful enough to destroy superconductivity (i.e. it has enough energy to destory Cooper pairs), and effective London penetration depth is attained from

$$\lambda_{eff}^2 = \frac{m^*c^2}{4\pi|\psi|^2 e^{*2}}.$$

λ_{eff} gives the value how deep the magnetic field can penetrate in to the superconductor.

Because we are now dealing with temperatures near T_c, thermal fluctuations

become an issue. Fluctuations are discussed in chapter 3.2 of this thesis, and it is worth mentioning that GL theory is a tool of choice when dealing with thermal fluctuations. Analysis of fluctuations using a microscopic model (e.g. BCS) is much more complicated.

3.1.3 1-dimensional superconductivity

Dimensionality of a superconductor can be determined by comparing its size to its coherence length ξ. If condition $d \ll \xi$ is satisfied, then the superconductor can be said to be one dimensional. Condition $d \ll \xi$ says that the wavefunction $|\psi|$ cannot vary across the wire. One can also assume condition $d \ll \lambda$, which allows to neglect the magnetic energies compared to kinetic energies. A critical difference between a one-dimensional and a bulk superconductor is that in the one-dimensional case resistivity can appear even below the critical temperature T_c. Close to critical temperature the finite resistance is caused by thermal fluctuations, or thermal phase slips, which can effectively destroy superconductivity for a short period of time in volume $A\xi$, where A is the cross-section of the wire. This leads to finite voltage and thus, finite resistivity. Probability of a phase slip event is $P_{ps} \sim \exp\left(-\frac{\Delta F_0}{\max\{k_B T, E_{ps}\}}\right)$, where ΔF_0 is energy necessary to create a single phase slip, while $k_B T$ is the contribution of thermal bath, and E_{ps} is the contribution of all other sources. In the temperature region $T \ll T_c$ thermal fluctuations die out and quantum fluctuations, usually called quantum phase slips, become dominant. Simply put, in an infinitely long wire there is always a finite probability that some part of the superconductor becomes normal for a short period of time due to fluctuations. These properties of one-dimensional superconductors are essential for this study. In 2- and 3-dimensional superconductors the fluctuations are undetectable in transport measurements since there is always another superconducting channel if one is destroyed. This prevents us from observing the phase slips, and thus fluctuations of the order parameter Δ. In sufficiently short nanowires it can be assumed that these phase slips are rare enough so that only one of them can be present at any given time. To study one-dimensional superconductors and phase slip processes, a wavefunction of the form

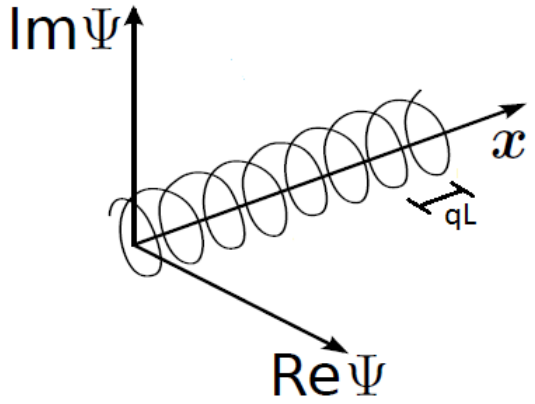

Figure 1: Complex current-carrying wavefunction. Picture from [4].

$$\psi(x) = |\psi(x)|e^{i\varphi(x)} \tag{15}$$

is needed. One needs to consider this in polar form in a plane perpendicular to x-axis. Solutions of this kind of functions are

$$\psi(x) = \psi_0 e^{iqx}$$

and are represented by helices of pitch $2\pi/q$ and radius ψ_0, see Fig. 1.

These are stationary solutions, which represent supercurrent flow and zero voltage (and with zero resistivity). If a voltage appears between the ends of the wire, the relative phase of the wavefunction changes by the Josephson relation

$$\frac{\mathrm{d}\varphi_{12}}{\mathrm{d}t} = \frac{2eV}{\hbar}, \tag{16}$$

where φ_{12} is a relative phase (of the two ends of the nanowire), e elementary charge, $\hbar$ reduced Planck constant and V voltage between the two ends of the wire. The total phase difference $\varphi_{12} = qL$, where L is the length of the wire, satisfies the Josephson relation. In uniform solution, the wavefunction looks like a helix moving along the x-axis with a radius of $|\psi|$ and phase being the

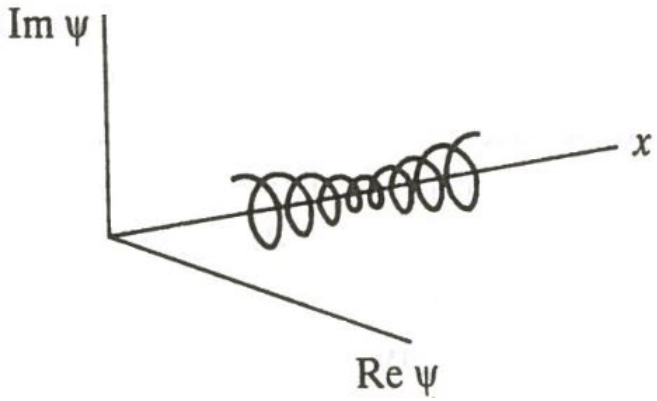

Figure 2: Schematic of phase slip event. Picture from [1].

same at every $2\pi/q$. In a non-uniform solution the helix tightens up until its radius reaches zero at some point, a phase slip occurs and the radius returns to $|\psi|$. This is demonstrated in Fig. 2

Locally Eq. (16) is equivalent to

$$\frac{\mathrm{d}v_s}{\mathrm{d}t} = \frac{eE}{m_e} \tag{17}$$

where v_s is the velocity of the supercurrent, E is electrical field inside the wire and m_e is a mass of an electron. This solution is steady even when $V > 0$ and $v_s < v_c$, v_c being the critical velocity of the quasi-particles. Higher velocity than v_c would yield enough kinetic energy for the Cooper pairs to break up. By demanding conservation of current, neglecting normal current and assuming that wavefunction has a form

$$\psi(x) = |\psi(x)|e^{i\varphi(x)},$$

then

$$|\psi(x)|^2\frac{\mathrm{d}\varphi}{\mathrm{d}x} = constant \propto I. \tag{18}$$

From Eq. (18) is it easy to see that if $|\psi|$ becomes small, $\frac{\mathrm{d}\varphi}{\mathrm{d}x}$ must become large. Figs. 1 and 2 demonstrate this observation.

Langer and Ambegaokar [5] found a path in function space between two uniform solutions with different number of turns in the helix shown in Fig. 1 with lowest free-energy barrier to overcome. They showed that the saddle-point free-energy increment ΔF_0 has a form

$$\Delta F_0 = \frac{\sqrt{2}}{3\pi} H_C^2 \cdot A\xi. \tag{19}$$

This is the case when no voltage is biased through the wire, meaning that the energy difference between the stationary states after a phase slip is zero. If a finite voltage is applied through the wire, phase slips to one direction (let's say $+2\pi$) become energetically favoured and they outnumber the -2π phase slips. In view of Eq. (16) (Josephson relation), energy difference between the state before and after a phase slip of magnitude 2π is

$$\delta F = \frac{h}{2e} I, \tag{20}$$

which is valid when a constant current source is used in an experimental setup. Picture 3 demonstrates the difference between applied voltage and zero voltage situations.

It is still necessary to introduce a so called attempt frequency Ω for a phase-slip event. If thermal fluctuations are only to be considered, then for mean a net phase-slip rate it can be derived to be

$$\frac{\mathrm{d}\varphi_{12}}{\mathrm{d}t} = 2\Omega \exp\left[-\frac{\Delta F_0}{k_B T}\right] \sinh\left(\frac{\delta F}{2k_B T}\right), \tag{21}$$

where Ω is an still an unknown prefactor. By substituting Eq.(20) to Eq.(21) and equating it to the Josephson frequency, we get

$$V = \frac{\hbar\Omega}{e} \exp\left[-\frac{\Delta F_0}{k_B T}\right] \sinh\left(\frac{hI}{4ek_B T}\right). \tag{22}$$

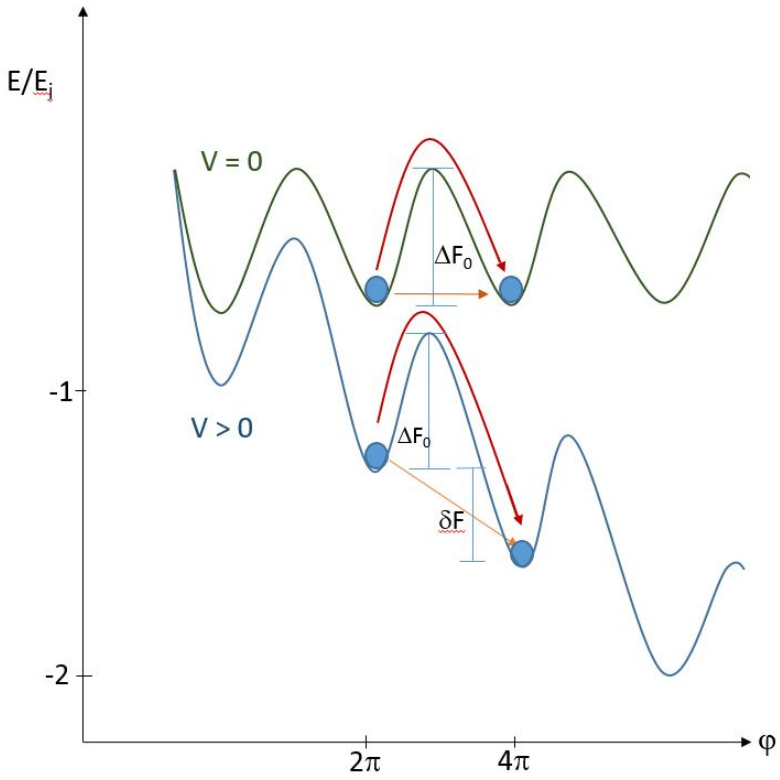

Figure 3: Phase slip events demonstrated. Green line represents the situation without a bias voltage, a case where $\delta F = 0$. Blue line represents the situation where finite bias voltage is applied. This is also known as 'tilted washboard potential'. Due to finite voltage, the phase slips to one direction become energetically favoured ($\delta F > 0$), and phase slips to that direction outnumber the ones to opposite direction. Orange lines represent a quantum tunneling (QPS) and red arrows represent a thermal phase slip (TAPS).

Applying Ohm's law and solving it for resistance, the result is

$$R = \frac{V}{I} = \frac{\pi\hbar^2\Omega}{2e^2k_BT}e^{-\frac{\Delta F_0}{k_BT}}. \tag{23}$$

This result applies only for very small currents (where $\sinh(x) \approx x$). The value of Ω is expected to be proportional to the length of the nanowire. The problem can also be examined by time-dependent Ginzburg-Landau theory (tdGL theory) and by it D. E. McCumber and B. I. Halperin [6] got a solution for the

unknown factor Ω, result being

$$\Omega(T) = \frac{L}{\xi}\sqrt{\frac{\Delta F_0}{kT}}\frac{1}{\tau_s},$$

where $\tau_s^{-1} = 8k(T_c - T)\pi\hbar$ is the characteristic relaxation rate of the superconductor in the GL theory. Indeed the initial guess about $\Omega \propto L$ ended up being true.

3.2 Phase slips

Phase slips can occur via two different mechanisms. First one is caused by the traditional thermal fluctuations which are dominant when the temperature of the superconductor is close to T_c (Eqs. (21),(22),(23)), and latter one is quantum mechanical, which is dominant far below the T_c region. To analyse this phenomenon in Josephson junction, usually one introduces a so called RCSJ (Resistively and Capacitively Shunted Junction) model, see Fig.4. I will go through the main points of this model, as it is important to understand it before going in to the details of a phase slip event. More detailed explanation can be found in [1]. An essential part of the RCSJ model is a so called 'tilted washboard potential', see Fig. 3. In this potential, phase slips happen when an electron moves from one potential minimum to another. When an electron does this by jumping over the potential barrier by acquiring enough thermal energy, it is called thermally activated phase slip, or TAPS in short. Another way is to tunnel through the barrier quantum mechanically. In this case we say that a quantum phase slip, or QPS, occurred. Schematics of this is shown in Fig. 3. It should be noted that in a conventional Josephson system formed of a static in space and time junction, schematics in Fig. 3 corresponds to the junction. In a homogeneous long nanowire a QPS is delocalized in space and time. However, if to simplify the discussion and consider short and narrow constriction, the probability of a QPS is higher in that location. Hence, the local description (Fig. 3) can be applied. Next I will go through the necessary details about RCSJ model, TAPS and QPS.

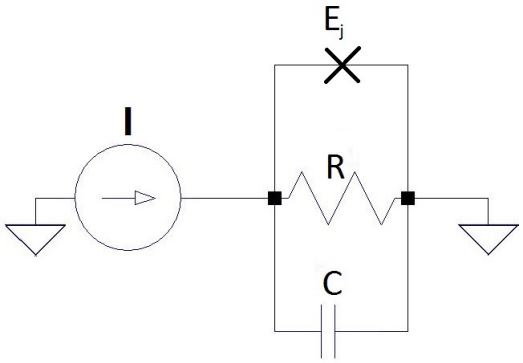

Figure 4: Circuit diagram of RCSJ model.

3.2.1 RCSJ model

The main reason to study RCSJ model is to gain information about the ac Josephson effect. The famous formula

$$I_s = I_c \sin(\gamma),$$

where I_s is supercurrent, I_c is critical current and γ is gauge-invariant phase difference of the two superconducting leads of the Josephson junction

$$\gamma = \Delta\varphi - \frac{2\pi}{\Phi_0} \int \vec{A} \cdot \vec{s}$$

is only sufficient when studying *zero* voltage dc properties of the junction. In the RCSJ model the physical Josephson junction is modeled by an ideal Josephson junction shunted by capacitance C and resistance R. It is worth noticing that C is capacitance between the electrodes, as capacitance to the ground can usually be ignored ($C_{junction} \ll C_{ground}$ so $C \approx C_{junction}$). At very low temperatures $R \approx R_N e^{\frac{\Delta}{k_B T}}$ where R_N is normal state resistance of the junction. This expression takes into account the dominant exponential temperature dependence arising from the freeze-out of quasi-particles at low temperature but not the weaker effect of the singular density of states at the gap edge in BCS theory [1]. In RCSJ model the time-dependence of the phase γ in the presence of bias current can be derived by equating the bias current with all three channels

of the RCSJ as usually with Kirchhoff's rules

$$I = I_{c_0}\sin(\gamma) + \frac{V}{R} + C\frac{\mathrm{d}V}{\mathrm{d}t}. \tag{24}$$

Here I_{c_0} is considered as a coefficient of $\sin(\gamma)$. It still describes a critical current, but it is *not* the observable critical current I_c that is measured. Usually $I_{c_0} > I_c$ due to thermal fluctuations. Thermal fluctuations are usually added to the equation by inserting $I = \langle I\rangle + \delta I(t)$ where $\delta I(t)$ describes the small fluctuations. Eliminating V from the above equation one gets second order differential equation for γ in the form of

$$\frac{\mathrm{d}^2\gamma}{\mathrm{d}\tau^2} + \frac{1}{Q}\frac{\mathrm{d}\gamma}{\mathrm{d}\tau} + \sin(\gamma) = \frac{I}{I_{c_0}}, \tag{25}$$

where $\tau = \omega_p t$ is a dimensionless time variable, $\omega_p = \sqrt{\frac{2eI_{c_0}}{\hbar C}}$ is the plasma frequency and $Q = \omega_p RC$ is known as the quality factor. Eq. 25 describes a particle moving in a tilted washboard potential mentioned above (Fig. 3). Tilted washboard potential is a mechanical analog based on equation of motion, Eq.(25). We end up in a similar motion when particle of mass

$$m = C\left(\frac{\hbar}{2e}\right)^2$$

subjected to a drag force

$$\left(\frac{\hbar}{2e}\right)^2 \cdot \frac{1}{R}\frac{\mathrm{d}\gamma}{\mathrm{d}t}$$

moves along the γ axis in an effective potential

$$U(\gamma) = -E_j\cos(\gamma) - \frac{\hbar I}{2e}\gamma. \tag{26}$$

From Fig. 3 it is easy to see that a characteristic energy scale of the model is the Josephson coupling energy $E_j = \hbar/2eI_{c_0}$. In the tilted washboard model, I_{c_0} has an easily understandable geometrical meaning. When $I = I_{c_0}$, washboard no longer has minima, but instead it becomes a downward slope that

has horizontal inflection points where the minima used to be. If the current is still increased, no stable points exist anymore. Noise, or thermal fluctuations, can now shift the energy of the system up or down by order $k_B T$. These fluctuations allow the particles to escape from the local minima that exists for I slightly smaller than I_{c_0}. In this event the phase of the wavefunction changes by $2\pi n$ or $-2\pi n$ depending on the direction where the particle is moving in the washboard potential. Hence the name is 'Thermally Activated Phase Slip'. Phase slip events are assumed to be relatively rare when the energy needed to create a single phase slip, ΔF_0, is larger than the "driving force" $\sim \Delta$. Then the probability of changing the phase by $2\pi n$ is

$$P_{n-ps} \sim \exp\left(-\frac{n \cdot \Delta F_0}{\Delta}\right),$$

hence cases with $n > 1$ are exponentially less probable compared to $n = 1$ phase slips.

3.2.2 Thermally activated phase slips (TAPS)

Theory describing TAPS was developed by J. Langer, V. Ambegaokar (1967), D. McCumber and B. Halperin (1970) [5, 6]. Langer-Ambegaokar-McCumber-Halperin theory, also known as LAMH theory, describes how finite resistance appears in thin nanowires due to thermally activated phase slips. Before going to details, we immediately conclude that LAMH theory is expected to break down when temperature T becomes really close to T_c as then the phase slip attempt frequency goes to zero. On the other hand, thermally activated phase slips die out at really low temperatures. Because we are dealing with one-dimensional superconductors the wavefunction ψ can vary only in x-direction. As mention before, tool of choice in LAMH theory is the time-dependent Ginzburg-Landau theory. One of the reasons being that in one dimension GL equation is analytically solvable.

As the main focus in this thesis does not lie in thermal phase slips, I will not go through the derivations. A More detailed explanation can be found in [5, 6] and main results can be recalled from chapter 3.1.3: TAPS attempt rate has a

form

$$\Omega(T) \exp\left(-\frac{\Delta F}{k_B T}\right)$$

where Ω is an attempt frequency

$$\Omega(T) = \frac{L}{\xi}\sqrt{\frac{\Delta F_0}{kT}}\frac{1}{\tau_s},$$

and ΔF_0 is free energy barrier for a (single) phase slip

$$\Delta F_0 = \frac{\sqrt{2}H_C^2}{3\pi} A\xi.$$

3.2.3 Quantum phase slips (QPS)

While TAPS is responsible for non-zero resistivity in temperatures slightly lower than T_c, the attempt frequency dies away in an exponential rate when the temperature is lowered. In the mK range, quantum phase slips become dominant over thermal phase slips and non-zero resistance still exists in the nanowire. In QPS procedure a macroscopis wavefunction tunnels through the free-energy barrier instead of hopping over it by thermal excitation. In short, in the mathematical derivation of QPS one starts with a partition function that explains statistical phenomena in the system and then assumes that quantum fluctuations exist in the system. Quantum phase slip events are then saddle point solutions of the effective action of this partition function (similar to TAPS model). Detailed derivation of QPS theory can be found in [7]. Next we go through the important results of this theory related to the thesis topic.

Assume the usual GL wavefunction form

$$\psi(x) = |\psi(x)|e^{i\phi(x)}. \tag{27}$$

As we are dealing with effectively one dimensional wires, the wavefunction is restricted in y and z-direction and $\psi(\vec{r}) \equiv \psi(x)$.

Since exponential function is never zero and the phase is considered to be a

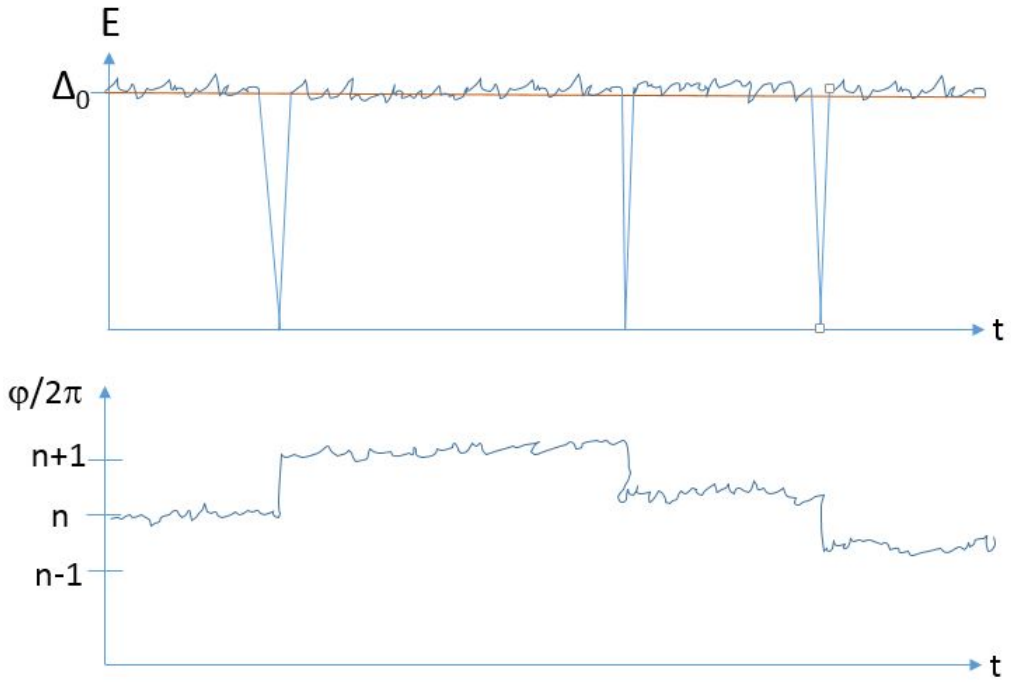

Figure 5: Schematic of fluctuations. Upper graph: Δ_0 (red line) denotes the bulk value of an energy gap. Blue line represents fluctuations of the gap. QPS causes superconductivity to break down momentarily, and this is shown in the picture as Δ dropping to zero for a short period of time. In addition to these QPSs, quantum fluctuations of the order parameter occur around the bulk value Δ_0. Lower graph: Blue line represents fluctuations of the phase φ. Phase is shifted $+2\pi$ or -2π when phase slip occurs. If voltage is not applied through the junction, $+$ and $-$ phase slips average out resulting to zero net change in phase.

continuous variable, then amplitude $|\psi(x)| = 0$ at some point. In other words, superconductivity is destroyed momentarily in the part where the phase slip occurs. See Fig. 5 for a schematic view of the process. Minimum volume of the fluctuating domain is $\xi(T) \cdot A$, where $\xi(T)$ is the temperature dependent GL coherence length and A is the cross-sectional area of the nanowire. $\xi(T)$ is defined as

$$\xi(T) = \xi(0) \left(1 - \frac{T}{T_c}\right)^{-1/2} \tag{28}$$

where

$$\xi(0) = \begin{cases} \xi_0 & \text{clean limit, } l \gg \xi_0 \\ 0.85\sqrt{\xi_0 l} & \text{dirty limit, } l \ll \xi_0, \end{cases} \tag{29}$$

where l is the normal state mean free path of an electron in the nanowire and $\xi_0 = w\frac{\hbar v_F}{k_B T_c}$ where v_F is the Fermi velocity and $w \approx 1$ is a constant, is Pippard's coherence length. From Josephson relation (16) we can then say that there is a voltage drop due to a phase change and this leads to a finite resistance. If the junction is not biased, then -2π and 2π phase slips have equal probability to occur. When a finite voltage over the junction is applied, phase slips to one direction become energetically favored and they no longer average to zero.

From LAMH theory we know that the resistance related to thermal phase slips is exponentially dependent on the height of the potential barrier

$$R(T) \propto \exp\left(-\frac{V_b}{k_B T}\right)$$

where V_b is the height of the barrier. In QPS, the same barrier is overcome by tunneling, and a similar type of relation is achieved

$$\nu \propto \exp\left(-\frac{V_b \tau}{\hbar}\right) \tag{30}$$

where ν is the attempt rate of tunneling and τ is characteristic time scale related to dynamics of tunneling. It should be of the same range as the time scale in superconductivity, so it is assumed to be $\tau \approx \hbar/\Delta$, reflecting just the uncertainty principle. If we have a finitely long nanowire, the QPS rate Γ_{QPS} is then

$$\Gamma_{QPS} = Be^{-S_{QPS}} \tag{31}$$

where

$$B \approx \beta \left(\frac{S_{QPS}}{\tau} \right) \cdot \left(\frac{L}{\xi(T)} \right)$$
$$S_{QPS} = \alpha \left(\frac{\frac{R_Q}{\xi(T)}}{\frac{R_N}{L}} \right), \tag{32}$$

where S_{QPS} is the effective QPS action, L is the length of the nanowire, $R_Q = {}^{h}/_{(2e)^2} \approx 6.4k\Omega$ resistance quantum, R_N effective shunting resistance coming from the wires and α,$\beta \approx 1$ are constants. Remembering that each phase slip creates a voltage, averaging it and defining effective resistance as $R_{eff} = {}^{\langle V \rangle}/_{I}$, we get

$$R_{eff} = \frac{\langle V \rangle}{I} = \underbrace{\Delta V_{QPS} \cdot \tau \cdot \Gamma_{QPS}}_{\langle V \rangle} \cdot \frac{1}{I} = \underbrace{\frac{I \cdot R_N \cdot \xi(T)}{L}}_{\Delta V_{QPS}} \cdot \frac{\tau \Gamma_{QPS}}{I} = R_N \frac{\xi(T)}{L} \cdot \tau \Gamma_{QPS}. \tag{33}$$

Contribution of QPS only in the effective resistance is

$$R(T) = b \frac{\Delta(T) S_{QPS}^2 L}{\xi(T)} e^{-2S_{QPS}} \tag{34}$$

where $b \approx 1$ is a constant with a suitable dimensions. For a "dirty limit" superconductor $l \ll \xi$, typical for lift-off fabricated nanostructures, which was the method in fabricating the measured samples. . Probability of QPS event has the same leading exponential dependence as Γ_{QPS} (Eq. (31)), and for a dirty limit superconductor can be reduced to a simple form:

$$P_{QPS} \propto \exp \left(\frac{-\gamma \sqrt{T_c^0} \sigma}{\rho_N} \right), \tag{35}$$

where σ is the effective diameter of the nanowire, T_c^0 is the critical temperature of a *bulk* SC, ρ_N is the usual normal state resistivity of the material and γ is a coefficient of proper dimensionality. From this formula we can already say that if a high QPS probability is wanted, nanowires should be as thin as possible,

chosen material should have low T_c^0 and high normal state resistivity. In this thesis, titanium is chosen as the material due to its relatively good properties in this regard. Idea is to maximize the amount of QPS events in the nanowires of different effective diameters σ so that behaviour of $\Delta(T_c,\sigma)$ can be studied.

3.3 Tunneling in SIS-junction

In 1962 B. D. Josephson made a prediction about a phenomenon which is today known as tunneling of Cooper pairs. In his famous papers [8,9] he stated that supercurrent can flow between two superconducting electrodes separated by a thin insulating layer. Supercurrent has a form

$$I_s = I_c \sin(\Delta\varphi), \tag{36}$$

where I_c is a critical current (the maximum current through the insulating layer without the presence of a voltage) and $\Delta\varphi$ is a difference in the phase of the GL wavefunction in the two electrodes. If a voltage difference is maintained between the electrodes (voltage biased measurement setup), the phase difference changes by

$$\frac{\mathrm{d}(\Delta\varphi)}{\mathrm{d}t} = \frac{2e}{\hbar}V, \tag{37}$$

which is identical to Eq.16. This results to an ac current of amplitude I_c with a frequency of $f = \frac{2eV}{\hbar}$. The energy hf then equals the amount of energy transferred by a Cooper pair from an electrode to another. This tunneling effect can happen in several cases, which are normally denoted by S-I-S (or SIS) and S-N-S (or SNS), N being 'normal metal', I 'insulator' and S stands for 'superconductor'. In this thesis, the focus is on SIS-junctions. From Eqs. (36) and (37) it is possible to solve the coupling free energy stored in the junction. The result is

$$F = C - E_J \cos(\Delta\varphi), \tag{38}$$

where C is a constant, $E_J \equiv \hbar I_c/2e$. It is easily seen that an energy minimum occurs when $\Delta\varphi = 0$, i.e. the phases of the wavefunctions are the same on both electrodes. The magnitude of a critical current tells us how strongly the phases are coupled through the insulating barrier, usually called a 'weak link'.

It is dependent on the chosen material and the thickness of the layer. The most common material for the insulating layer is aluminum oxide (AlO_x) due to its practicality.

Derivation of current-voltage characteristics of an SIS tunnel junction is here done with second quantization notations and for that new quasiparticle operators are introduced. These are defined as follows:

$$\begin{aligned} c_l^\dagger &= u_l \gamma_l^\dagger + v_l^* \gamma_l \\ c_l &= u_l^* \gamma_l + v_l \gamma_l^\dagger \\ c_r^\dagger &= u_r \gamma_r^\dagger + v_r^* \gamma_r \\ c_r &= u_r^* \gamma_r + v_r \gamma_r^\dagger. \end{aligned} \tag{39}$$

Here γ operators are creation- and annihilation operators of quasiparticles that tunnel through the barrier, r and l indexes denote which side of the barrier particle is tunneling. c operators are the regular electron creation- and annihilation operators. Hamiltonian for the problem has a form $\hat{H} = \hat{H}_L + \hat{H}_R + \hat{H}_T$ where $\hat{H}_L$ describes the quasiparticles on the left component of the junction, $\hat{H}_R$ on the right component and $\hat{H}_T$ is the so called tunneling Hamiltonian. $\hat{H}_T$ transfers quasiparticles between the electrodes. Tunneling Hamiltonian has a form

$$\hat{H}_T = \sum_{l,k,s} = \left(T_{lr} c_r^\dagger c_l + T_{lr}^* c_l^\dagger c_r \right) \tag{40}$$

where T_{lr} is a phenomenological tunneling matrix element and s spin. T_{lr} gives the probability of a tunneling between the electrodes and details of the insulating barrier (material, thickness etc.) are absorbed to these matrix elements. Substituting Eq. (39) to the tunneling Hamiltonian gives

$$\hat{H}_T = \sum_{l,r} T_{lr} \left(u_r u_l \gamma_r^\dagger \gamma_l + u_r v_l \gamma_r^\dagger \gamma_l^\dagger + v_r u_l \gamma_r \gamma_l + v_r v_l \gamma_r \gamma_l^\dagger \right) + \text{herm. conj.} \tag{41}$$

Superconducting ground state is known to be citetinkham

$$|\psi_G\rangle = \prod_{\vec{k}=\vec{k}_1,\ldots,\vec{k}_M} \left(u_{\vec{k}} + v_{\vec{k}} c_{\vec{k},\uparrow}^* c_{-\vec{k},\downarrow}^* \right) |\phi_0\rangle \tag{42}$$

where $|\phi_0\rangle$ is the vacuum state with no particles present. We now denote the ground state on left electode as $|\phi_L\rangle$ and $|\phi_R\rangle$ on the right. Excited states are denoted by $|l\rangle = \gamma_l^\dagger|\phi_L\rangle$ and $|r\rangle = \gamma_r^\dagger|\phi_R\rangle$ respectively. Now the matrix element options that lead to transfer of one Cooper pair across the junction are.

$$T_{lr}u_l u_r \left\langle \phi_L,r|\gamma_r^\dagger\gamma_l|l,\phi_R \right\rangle + T_{lr}^\dagger v_l v_r \left\langle \phi_l,r|\gamma_l\gamma_r^\dagger|l,\phi_R \right\rangle, \quad \Delta E = E_l - (E_r + eV) \tag{43}$$

can be identified to be a simple quasiparticle tunneling (qp),

$$T_{lr}u_r v_l \left\langle l,r|\gamma_r^\dagger\gamma_l^\dagger|\phi_L\phi_R \right\rangle + T_{lr}^\dagger v_r u_l \left\langle l,r|\gamma_l^\dagger\gamma_r^\dagger|\phi_L\phi_R \right\rangle, \quad \Delta E = eV - (E_l + E_r) \tag{44}$$

as a Cooper pair breaking current (pb),

$$T_{lr}v_r u_l \langle \phi_L,\phi_R|\gamma_r\gamma_l|l,r\rangle + T_{lr}^\dagger u_r v_l \langle \phi_L,\phi_R|\gamma_l\gamma_r|l,r\rangle, \quad \Delta E = (E_l + E_r) - eV \tag{45}$$

as a recombination current (r) and By applying

$$\left\langle \gamma^\dagger\gamma \right\rangle = f = \left(\exp\left[\frac{E}{K_B T}\right] + 1 \right)^{-1}$$

and

$$\left\langle \gamma\gamma^\dagger \right\rangle = 1 - f,$$

we can solve thermal average for all currents individually

$$\begin{aligned}
\Gamma_{L\to R}^{qp} &= \frac{2\pi}{\hbar}\sum_{l,r}|T_{lr}|^2 f_l(1-f_r)\cdot\delta(E_l - E_r - eV) \\
\Gamma_{R\to L}^{qp} &= \frac{2\pi}{\hbar}\sum_{l,r}|T_{lr}|^2 f_r(1-f_l)\cdot\delta(E_r - E_l + eV) \\
\Gamma^{pb} &= \frac{2\pi}{\hbar}\sum_{l,r}|T_{lr}|^2 (1-f_l)(1-f_r)\cdot\delta(eV - (E_l + E_r)) \\
\Gamma^{r} &= \frac{2\pi}{\hbar}\sum_{l,r}|T_{lr}|^2 f_l f_r\cdot\delta(E_l + E_r - eV).
\end{aligned} \tag{46}$$

Here $\delta(x)$ is the regular Dirac delta function. Notice that the coherence factors u_l,u_r,v_l,v_r drop out due to electron-hole symmetry. Result for total quasiparti-

cle current is then

$$\begin{aligned} I_{tot} &= e\left(\Gamma^{qp}_{L\to R} - \Gamma^{qp}_{R\to L}\right) + e\left(\Gamma^{pb} - \Gamma^{r}\right) \\ &= \underbrace{\frac{2\pi e}{\hbar}\sum_{l,r}|T_{lr}|^2(f_l - f_r)\delta(E_l - E_r - eV)}_{I_1} + \underbrace{\frac{2\pi e}{\hbar}\sum_{l,r}|T_{lr}|^2(1 - f_l - f_r)\delta(E_l + E_r - eV)}_{I_2}. \end{aligned} \tag{47}$$

This can be calculated by changing sums to integrals and adding related DOS to the function. Superconducting density of states can be obtained as follows. As there is one-to-one correspondence between γ and c operators, we must have

$$N_s(E)\mathrm{d}E = N(\xi)\mathrm{d}\xi. \tag{48}$$

We are interested in energies ξ (not to be confused with the coherence length) that are just above Fermi energy, we can make approximate the normal state density of states $N(\xi)$ to be constant, $N(\xi) = N(0)$. Recalling Eq. (7) this approximation leads to a very simple result

$$\frac{N_s(E)}{N(0)} = \frac{\mathrm{d}\xi_{\vec{k}}}{\mathrm{d}E_{\vec{k}}} = \frac{\mathrm{d}}{\mathrm{d}E_{\vec{k}}}\sqrt{E^2_{\vec{k}} - \Delta^2} = \begin{cases} \frac{E_{\vec{k}}}{\sqrt{E^2_{\vec{k}} - \Delta^2}} & (E > \Delta) \\ 0 & (E < \Delta) \end{cases} \tag{49}$$

and same for quasiholes if $\frac{\mathrm{d}|\xi|}{\mathrm{d}E_{\vec{k}}}$. From above formula it is easy to see that the superconducting DOS diverges as $E = \Delta$. Schematic of the DOS is shown in Fig. 6

Now that we have superconducting DOS introduced, it is possible to calculate the current through SIS-junction. Changing sums to integrals

$$\sum_{l,r} \to \iint \mathrm{d}E_l \mathrm{d}E_r N_L(0) N_R(0) N_s(E_l) N_s(E_r) \tag{50}$$

we get

$$I_{SIS} = I_1 + I_2 \tag{51}$$

where

$$I_1 = \frac{2\pi e}{\hbar}|T_{lr}|^2 N(0)^2 \int_{-\infty}^{\infty} \mathrm{d}\epsilon \, (f(\epsilon - eV) - f(\epsilon)) \, \frac{|\epsilon - eV|}{\sqrt{(\epsilon - eV)^2 - \Delta^2}} \frac{|\epsilon|}{\sqrt{\epsilon^2 - \Delta^2}}$$

$$I_2 = \frac{2\pi e}{\hbar}|T_{lr}|^2 N(0)^2 \int_{-\infty}^{\infty} \mathrm{d}\epsilon \, (f(-\epsilon + eV) - f(\epsilon)) \, \frac{|eV - \epsilon|}{\sqrt{(eV - \epsilon)^2 - \Delta^2}} \frac{|\epsilon|}{\sqrt{\epsilon^2 - \Delta^2}}. \tag{52}$$

Noticing that $1 - f(-x) = f(x)$ we get

$$I_{SIS} = \frac{4\pi e}{\hbar}|T|^2 N(0)^2 \int_{-\infty}^{\infty} \mathrm{d}\epsilon \, [f(\epsilon - eV) - f(\epsilon)] \, \frac{|\epsilon - eV|}{\sqrt{(\epsilon - eV)^2 - \Delta_1^2}} \cdot \frac{|\epsilon|}{\sqrt{\epsilon^2 - \Delta_2^2}}. \tag{53}$$

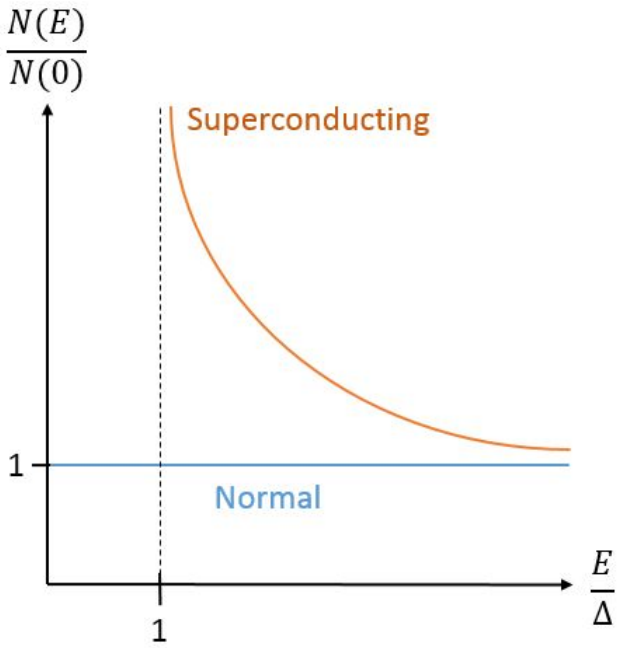

Figure 6: Schematics of the density of states of the normal metal and a superconductor. Blue line represents the normal metal DOS, and the orange curve represents superconducting DOS. Superconducting DOS diverges at $\frac{E}{\Delta}$ and approaches normal metal DOS as the energy of the quasiparticles increase.

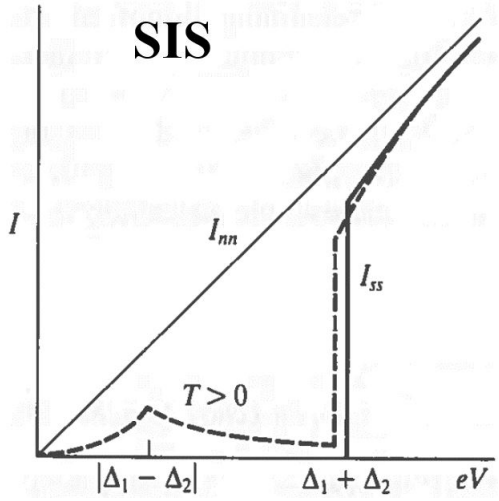

Figure 7: $I(V)$-characteristics of an SIS-junction. Picture from [1].

$I(V)$-characteristics of an SIS-junction is shown in Fig. 7. This is a general formula for junctions in which the weak-coupling approximation applies. If SC materials are not the same, i.e. $\Delta_1 \neq \Delta_2$, an extra feature appears around $eV = |\Delta_1 - \Delta_2|$ when $T > 0$. This happens because the bias voltage provides just enough energy for the quasi-particles in the peak of the density of states at, for example Δ_1, to tunnel to peak of DOS of Δ_2. If $\Delta_1 = 0$, then the solution reduces to current for NIS-junction

$$I_{NIS} = \frac{4\pi e}{\hbar}|T|^2 N(0)^2 \int_{-\infty}^{\infty} \mathrm{d}\epsilon \, [f(\epsilon - eV) - f(\epsilon)] \cdot \frac{|\epsilon|}{\sqrt{\epsilon^2 - \Delta_2^2}}. \tag{54}$$

When studying the energy gap Δ, it is usually advisable to study an SIS-junction. This is due to the two distinct features observed in an SIS-junction which makes it simple and more accurate method compared to studying an NIS-junction, because in a real measurement setup $T > 0$ condition always applies, causing the peak to appear in the measured $I(V)$-characteristics. This way one can observe 2 features and we have two 2 unknown variables, leading to an easily solvable group of equations. This does not necessarily apply in

one dimensional case, as will be seen in the upcoming chapters of this thesis.

4 Experiments

Objective of the experimental part is to fabricate the appropriate samples enabling experimental determination of the impact of quantum fluctuations on the amplitude of the superconducting order parameter. SIS-junctions were studied in this thesis. Each sample had the same basic structure, but many parameters were varied throughout the fabrication process to get the best possible quality for the junctions. Each sample has a relatively wide (150-200nm depending on sample) aluminum wire connecting the six smaller nanowires perpendicular to the wider wire, see Fig. 8.

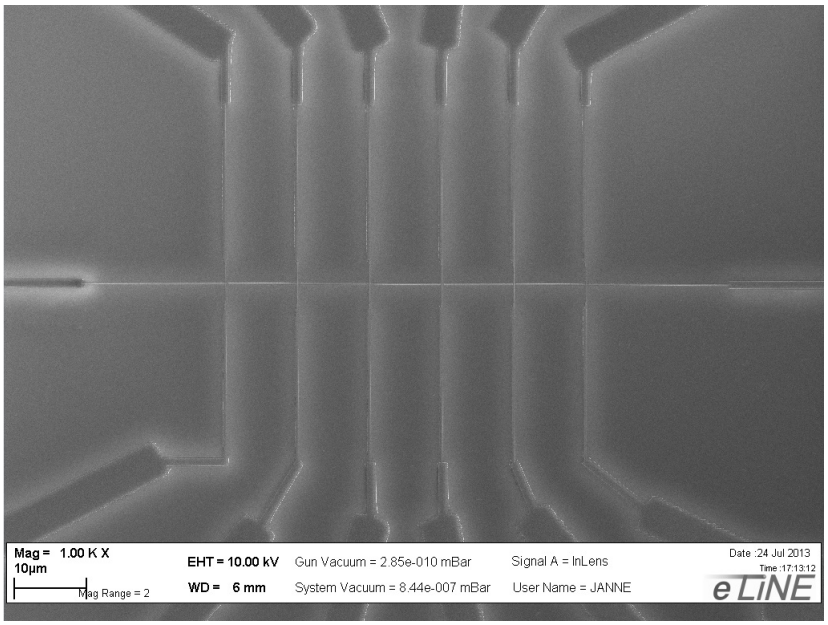

Figure 8: Scanning Electron Microscope (SEM) image of the measured SIS-structure. 6 titanium nanowires are overlapping the aluminum wire through SIS-junctions.

At crossings of these wires there is an SIS-junction. Notable differences in fabrication process were in material evaporation. Regular and shadow evaporation methods were used. Another highly varied parameter was the insulating layer: amount of aluminum, pressure and time used in oxidizing it. Goal was to get highly ohmic junctions to get rid of Josephson current. Two samples were fabricated with Al-AlO_x-Ti junctions and in one sample there is 2 nm of palladium evaporated on top of AlO_x.

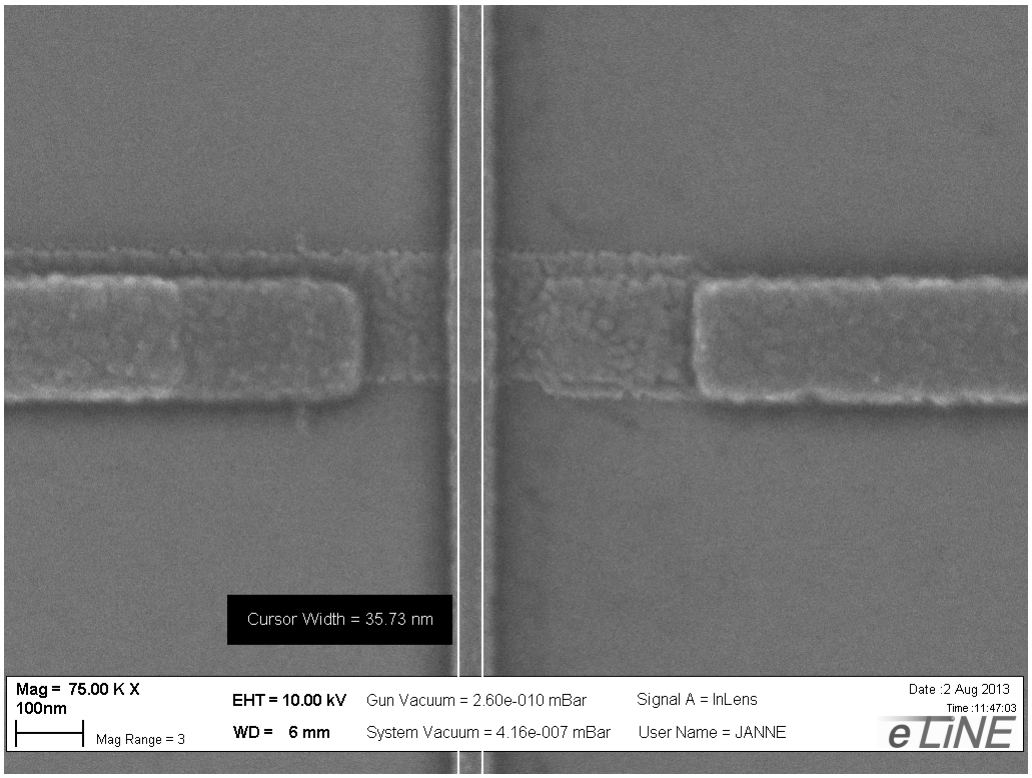

Figure 9: SEM image of a typical Al-AlO_x-Ti SIS-junction. Horizontal wire is the aluminium wire, and vertical wire is the titanium one.

4.1 Sample fabrication

Samples were fabricated using a conventional e-beam lithography method. Samples were cleaned by reactive ion etching using low energetic oxygen plasma.

Narrow mask down to sub 25 nm width were drawn and materials were deposited in ultra high vacuum (UHV) chamber at 10^{-9} mbar pressure. Several different types of structures were patterned to test which way would give the best quality for the junctions. conventional shadow evaporation technique gave satisfying quality for the nanowires and the insulating layer. Over 100 kΩ ohmic resistance was obtained, which is already enough to suppress undesired Josephson current at low bias $eV \ll \Delta$.

One can also use different angles to successfully evaporate metals to form a junction. Downside in this method is that titanium has to be evaporated from non-zero angle, which degrades the quality of the deposited material. This is because in undercut of the photoresist layer there is always some residuals left on the silicon surface which adds defects to the titanium layer. Another problem is that residual moisture is harder to clean in the undercut section. In the worst case scenario, titanium will not exhibit a superconducting transition. On the other hand, if there are no shadows to prevent aluminum deposition, insulating layer is easier to fabricate since aluminum is evaporated everywhere and oxidized, removing the chance of a metal-metal contact.

4.2 Measurement setup

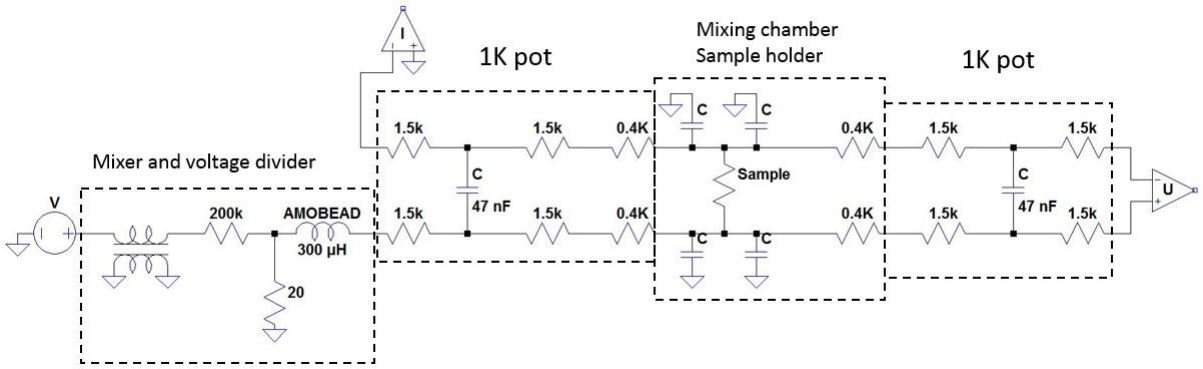

Figure 10: Four-probe measurement setup used in the measurements.

All samples were measured in a ^{3}He/^{4}He dilution refrigerator with a stable base temperature of $T = 26$ mK. Cryostat was placed in an electromagnetically shielded room along with analog current and voltage amplifiers. RF filtering and lock-in techniques were used in the measurements. All $R(T)$- and $I(V)$-measurements were done by standard dc measurement methods with ac modulation. 4-probe measurement setup was used in $I(V)$-measurements to eliminate the contribution of probes. $R(T)$-measurements were done with the (traditional) 2-probe setup. The contribution of the measuring probes (including high resistive RF filters) was subtracted from the data afterwards.

4.3 Analysis

4.3.1 $R(T)$-measurements

Total of 6 junctions and 8 wires were studied in these measurements. $R(T)$-measurements of the nanowires tell us directly about the $T_c(\sigma)$ dependence. Results are shown in Figs. 11,12,14. The transition at $T_c \approx 400$ mK related to the contribution of the thicker sections of the structure becoming superconducting is removed. The $R(T)$ data agrees well with earlier experiments on QPS effect in titanium nanowires [10, 11]

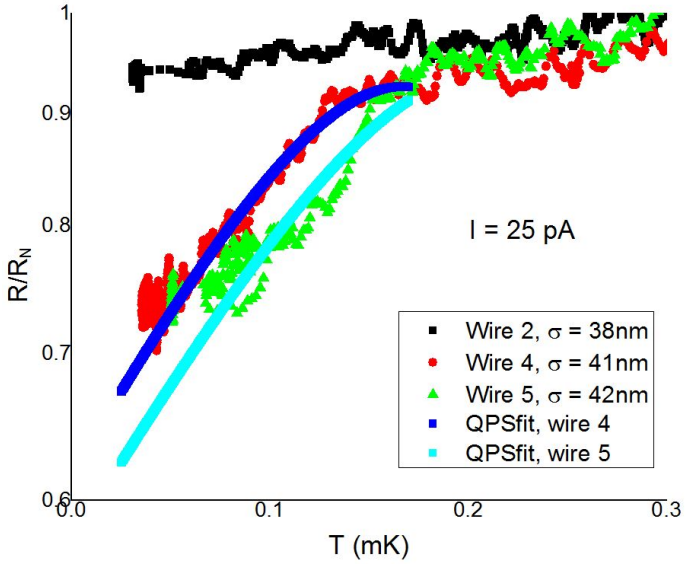

Figure 11: $R(T)$-dependance of several nanowires of sample 72 with different effective diameters σ. Blue and cyan solid lines correspond to QPS fittings (Eq. (34)).

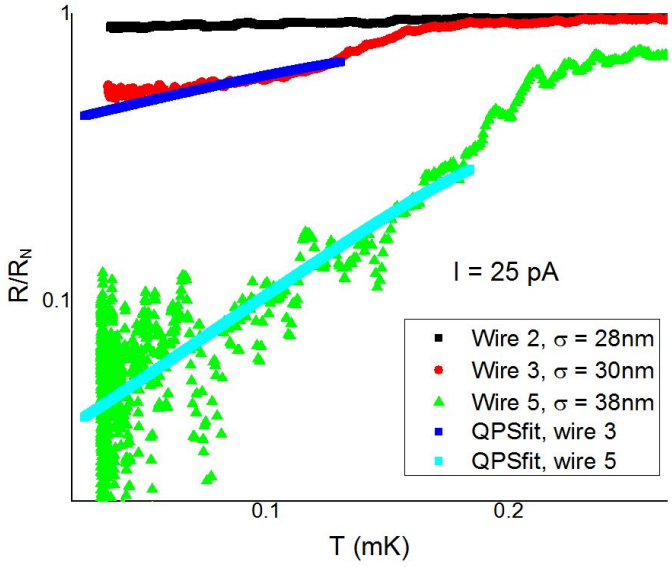

Figure 12: $R(T)$-dependence of several nanowires of sample 74 with different effective diameters σ. Blue and cyan solid lines correspond to QPS fittings (Eq. (34)).

In Figs. 11 and 12 the trend is clear. Thinner wires have higher resistance and in both plots the thinnest wire does not show superconducting transition at all. One should pay attention to the values of σ and R in the first two samples. In the first one the wire with effective diameter $\sigma = 38$ nm does not exhibit a superconducting transition, but wires with $\sigma = 41$ nm and $\sigma = 42$ nm do show at least some trend. In the second sample the wire with $\sigma = 28$ nm does not have a transition while wires with $\sigma = 30$ nm and $\sigma = 38$ nm do. One explanation for this could be the evaporation process, as the quality of the titanium can differ in each evaporation. Evaporation rate and quality of the vacuum highly affect the outcome of this process. If this is the case, it indicates that in the first evaporation the material itself had a poor quality compared to the second evaporation. This again can come from several reasons: material itself, vacuum level, evaporation rate, how well the plasma cleaning succeeded and how well the aluminum was oxidized. Parameters used in the evaporation process are shown in Table 1.

Table 1: Parameters of the material deposition in the UHV chamber

Sample	Material	Thickness (nm)	p (mbar)	deposition rate $\left(\frac{\text{Å}}{\text{s}}\right)$
72	Al	24	$4 \cdot 10^{-8}$	1.0
72	Ti	35	$5 \cdot 10^{-9}$	0.8
74	Al	30	$2 \cdot 10^{-8}$	1.0
74	Ti	30	$6 \cdot 10^{-9}$	1.0

Values for both samples look quite similar, so the reason for this difference lies somewhere else. Sadly, cleanliness of the silicon surface under the deposited material cannot be analysed. Calculating the resistivity of each nanowire gives information about the quality of the material. Results are shown in Table 2.

Clearly wires in sample 72 have a lot higher resistivities compared to sample 74 (and 82). Combining the information from Tables 1 and 2 several conclusions can be made: the cleaning of the silicon surface was more successful in sample

Table 2: Resistivities of nanowires

Sample	Wire	$\rho(\Omega \cdot \mathrm{nm})$
72	2	2796
72	4	2576
72	5	2463
74	2	1410
74	3	1255
74	5	923
82	2	1653
82	4	1411

74 than on 72, there was some moisture left on the surface of the silicon or the grain-size is just smaller in sample 72 causing more scattering of electrons at the boundaries of the grains. These are most probable reasons that could cause the resistivity difference.

Effect of the QPS phenomenon related to the broadening of the $R(T)$ superconducting transition in nanowires was also studied. Figures 11 and 12 show QPS fittings for the two wires in each sample that exhibit a clear transition. Formula used for fitting has a form similar to Eq. (34)

$$\frac{R_{QPS}(T)}{R_N} = \left(\frac{\Delta(T)}{\Delta(0)}\right) \cdot \frac{L \cdot S_{QPS}^2}{\xi(T)} e^{-2S_{QPS}} \tag{55}$$

where

$$S_{QPS} = A \cdot \frac{R_Q L}{R_N \xi(T)}, \qquad \xi = \sqrt{\frac{\xi_0 l}{1 - \frac{T}{T_c}}}, \tag{56}$$

and

$$\Delta(T) = 1.76 \cdot \Delta(0) \left(1 - \frac{T}{T_c}\right)^{\frac{1}{2}} \left(\frac{T}{T_c}\right)^{\frac{1.04}{4}} \tag{57}$$

and ξ_0 is Pippard's coherence length, l is the mean free path and $A \approx 0.3$ is numerical constant. The parameters of the fits are shown in Table 3 and Eq. 57 is plotted in Fig. 13. There are several limitations to this model: It works only in temperatures well below T_c and the QPS rate should be small compared to the energy gap $|\Delta|$, i.e. $S_{QPS}^{-1} \ll 1$. QPS rate of each of the wires are listed in the

Table 4.

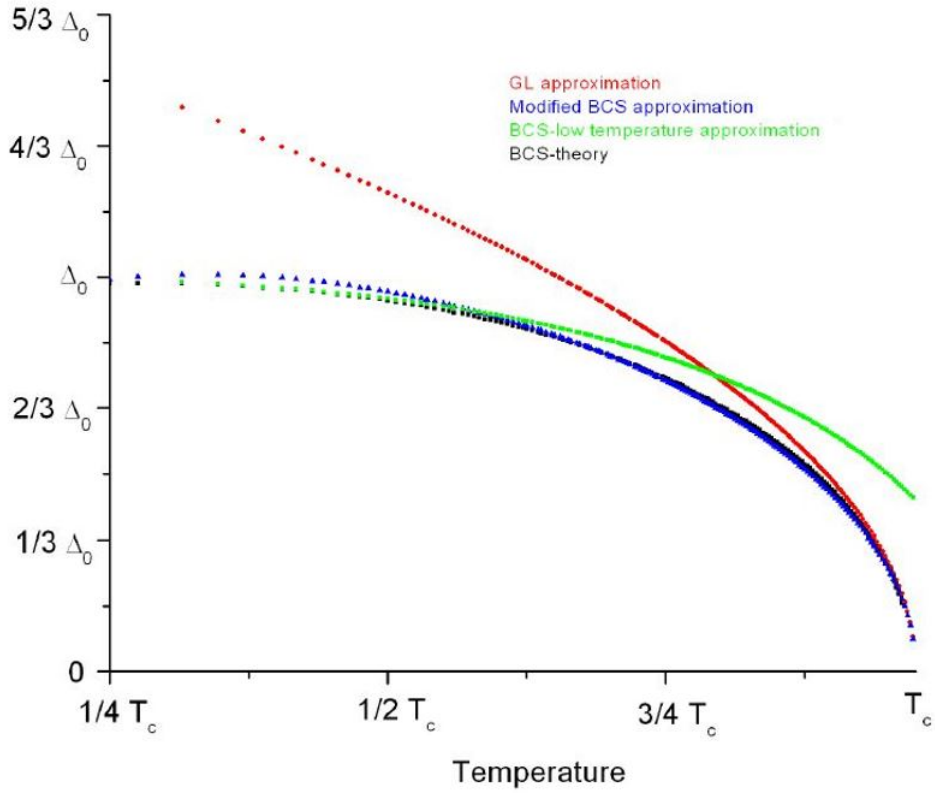

Figure 13: Different approximations for the temperature dependence of the energy gap Δ. Modified BCS approximation Eq. (57 (blue dots) is used in QPS fits (Eq. (34)). Fig. taken from [12]

Wire 5 of sample 74 (Fig.12) clearly has the best correspondence between the theory [7] and experiment. This can be accounted to the fact that wire 5 has highest value of S_{QPS}, thus satisfying the condition $S_{QPS}^{-1} \ll 1$ better than the other wires. In practice this means that the wires with small relative resistance drop exhibit a lot of phase slips which destroy superconductivity. This again violates the assumption of QPS events being fairly rare, thus violating the model applicability in those cases. For the same reason QPS fit was not done for the wires which do not have a clear transition at all.

Table 3: Parameters of QPS fits

Sample	Wire	T_c(mK)	A
72	2		
72	4	300	0.378
72	5	350	0.330
74	2		
74	3	300	0.249
74	5	250	0.470

Table 4: QPS rate in each of the fits in Figs. 11 and 12

Sample	Wire	$S_{QPS}(T = 0)$
72	2	3.16
72	4	2.54
72	5	2.67
74	2	3.06
74	3	2.90
74	5	4.63

$R(T)$ measurements of sample 82 can be seen in Fig. 14. Addition of 2 nm layer of palladium greatly decreases the critical current of the wires. Only one transition is seen which indicates that the wider parts of the sample become superconducting around $T \approx 200$ mK, while pure titanium has a $T_c \approx 400$ mK. Nanowire itself presumably stays in the normal state. From these results two things can be stated immediately. Firstly ohmic resistance of the nanowire increased greatly due to the palladium layer. That was made to prevent titanium of reacting with aluminum oxide, and seemingly it works in that part. The second conclusion is that it lowers the T_c of titanium drastically.

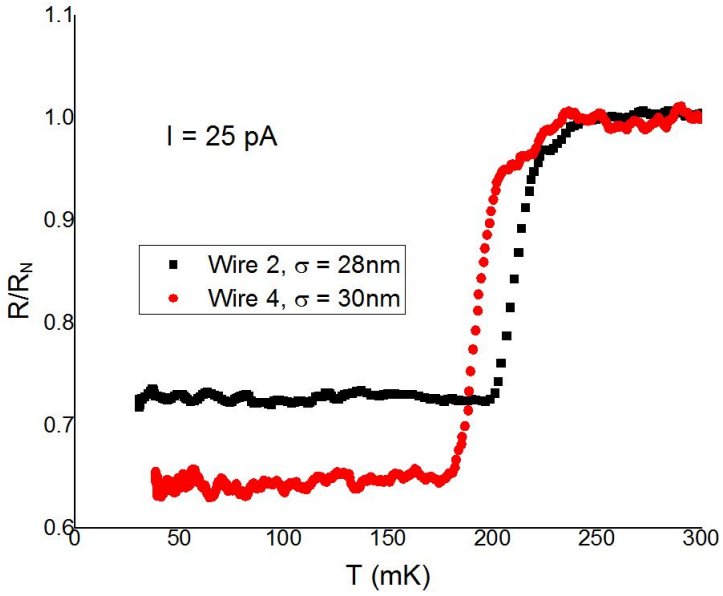

Figure 14: $R(T)$-dependence of several nanowires of sample 82 with different effective diameters. 2 nm layer of palladium is evaporated between AlO_x and Ti nanowire

4.3.2 $I(V)$-measurements

In this section we study $I(V)$ and $\frac{dI}{dV}(V)$ dependencies of the SIS junctions between Ti nanowires, and the aluminum (common) electrode (see Figs. 8 and 9). Notation "junction X" corresponds to a SIS junction between wire X and the aluminum wire. Figure 15 shows the $I(V)$-characteristics of the same SIS-junction at different temperatures. Corresponding differential conductance $\frac{dI}{dV}(V)$ of the same junction is shown in Fig. 16. Wire 4 ($\sigma = 41nm$) exhibits a weak resistance drop in $R(T)$ data. The $I(V)$ and $\frac{dI}{dV}(V)$ characteristics demonstrate the appearance of Josephson current, and a distinct feature at point $eV = |\Delta_{Al} - \Delta_{Ti}| = 0.05$ mV. Results can be seen in Figs. 17 and 18.

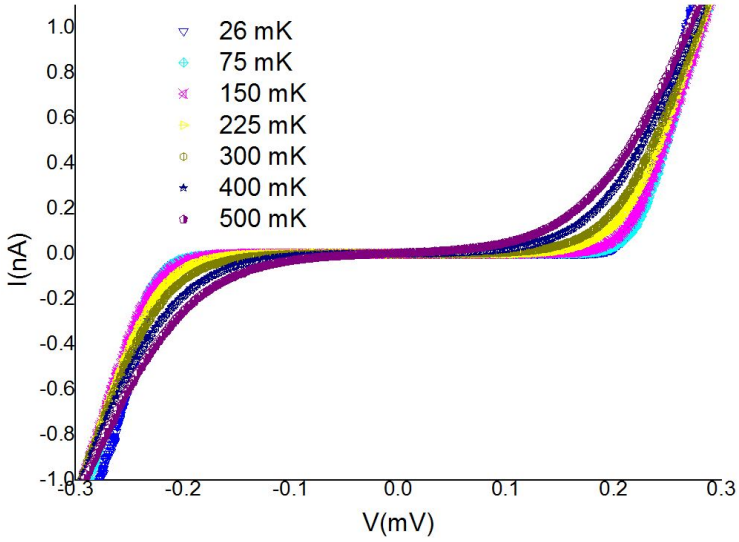

Figure 15: $I(V)$-characteristics of the SIS-junction of sample 72, between wire 2 and the aluminum electrode, at various temperatures. No measurable Josephson current is detected

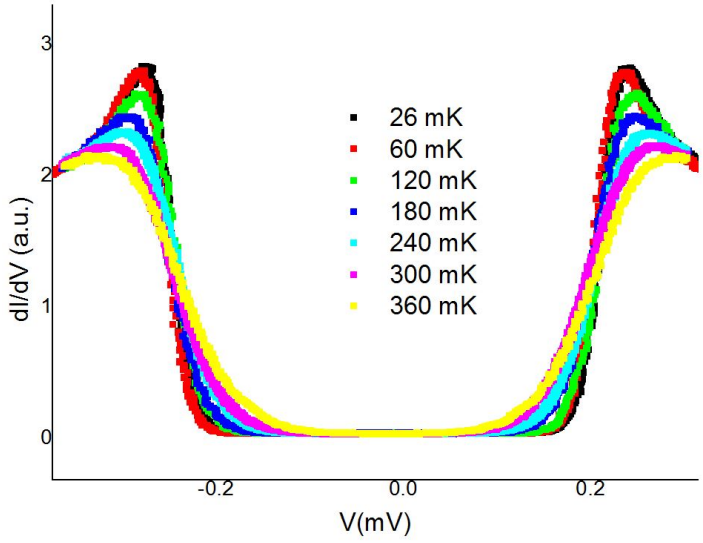

Figure 16: $\frac{\mathrm{d}I}{\mathrm{d}V}(V)$-characteristics of the SIS-junction of sample 72, between wire 2 and the aluminum electrode at various temperatures. No measurable Josephson current is detected

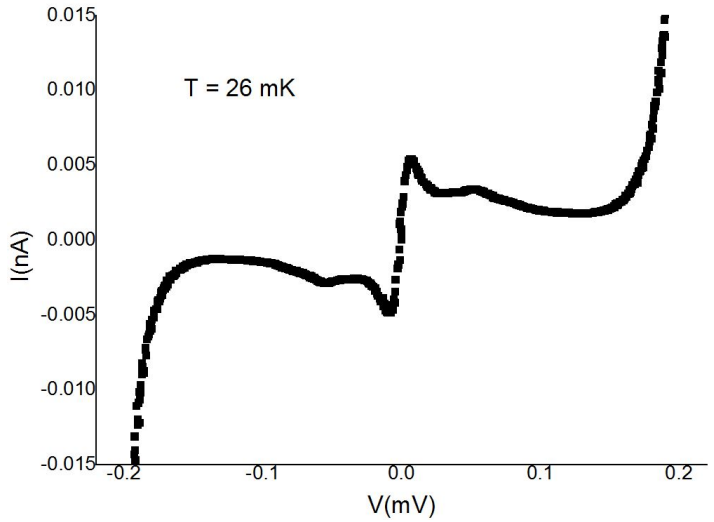

Figure 17: $I(V)$-characteristics of SIS-junction in sample 72, between wire 4 and the aluminum electrode at temperature $T = 26$ mK. Measurably high Josephson current is detected at low bias $eV = 7\ \mu$ V

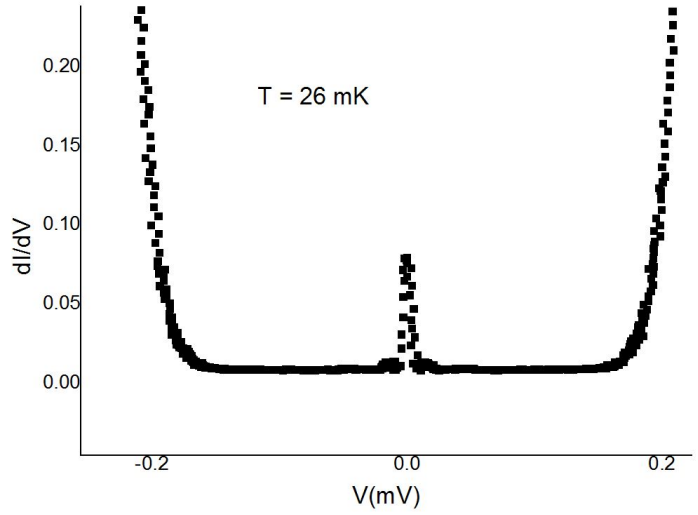

Figure 18: $\frac{\mathrm{d}I}{\mathrm{d}V}(V)$-characteristics of SIS-junction in sample 72, between wire 4 and the aluminum electrode at temperature $T = 26$ mK. Measurably high Josephson current is detected.

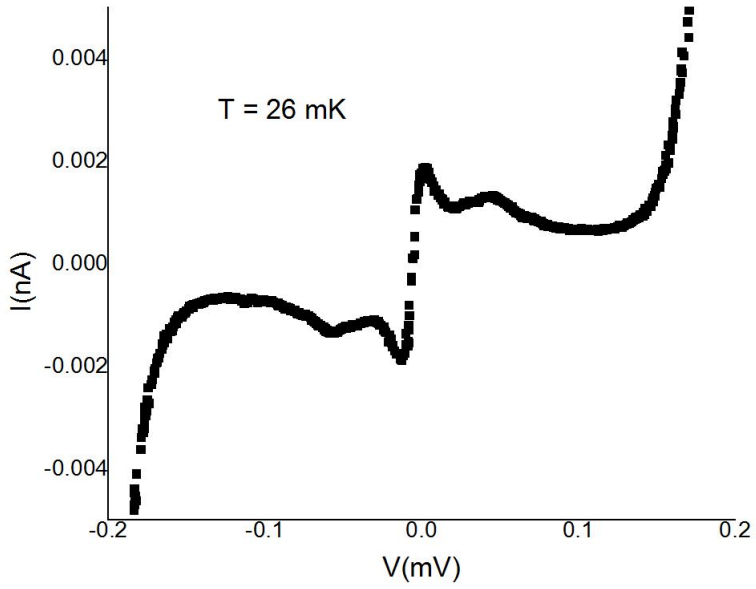

Figure 19: $I(V)$-characteristics of an SIS-junction of sample 72, between wire 5 and the aluminum electrode. Notice the scale difference compared to Fig. 17

The same phenomenon happens in junction 5 (Fig. 19). Difference in the Josephson current comes from the difference in the tunnel resistance ($R_T = \left(\frac{\mathrm{d}I}{\mathrm{d}V}\right)^{-1}$ when $V \gg \frac{\Delta}{e}$) of SIS-junctions 2 and 3, $R_{T_2} \approx 83\ \mathrm{k}\Omega < R_{T_3} \approx 143\ \mathrm{k}\Omega$.

SIS junctions of sample 74 exhibit similar behaviour as expected from the $R(T)$ data (Fig. 12). $I(V)$-characteristics of all three junctions as plotted in Fig. 20. Wire 2 does not exhibit a superconducting $R(T)$ transition and thicker wires do (Fig. 20): wire 3 shows a really small Josephson current, 5 has a noticeable one. Notice the significant feature at $eV = |\Delta_{Al} - \Delta_{Ti}| \approx 50\ \mu$V regime in junction 5, which is much larger than the one observed in the wire 5 of sample 72 . Reason for this feature is not known.

For further analysis of $I(V)$-characteristics and especially fluctuations of Δ, one should study and compare $\frac{\mathrm{d}I}{\mathrm{d}V}$ data. After initial measurements sample 72 was sputtered, i.e. the diameter of the nanowires was reduced by low-energetic ion milling, and measured again. Results are plotted in Figs. 21, 22 and 23. Differences in asymptotic values of $\frac{\mathrm{d}I}{\mathrm{d}V}(V \gg (\Delta_{Al} + \Delta_{Ti}))$ in the same sample

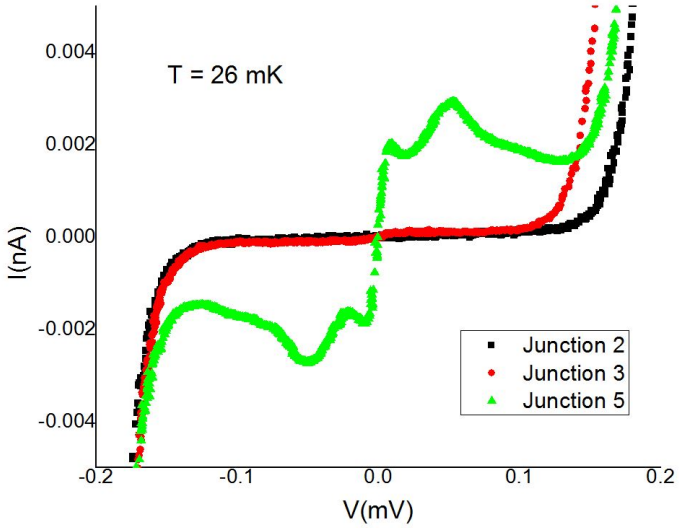

Figure 20: $I(V)$-characteristics of SIS-junctions of sample 74. Junctions are formed between the aluminum electrode and the titanium wires 2, 3 and 5.

arise from the difference in the tunneling resistance R_T and the difference in resistivity ρ between the samples (see Table 2). In sample 72 a large difference in the width of the peak can be noticed in wire 2 compared to wires 4 and 5 which are of almost of the same shape. The rate of quantum fluctuations exponentially increases as the diameter of the wire decreases. Comparison of the sample 72 before and after sputtering supports this observation. The expectation value of the energy gap in titanium nanowires $\langle \Delta_{Ti} \rangle$ are determined from the position of the $|\Delta_{Ti} + \Delta_{Al}|$ peculiarity of the experimental $I(V)$'s. The corresponding values of $\langle \Delta_{Ti} \rangle$ in different nanowires are plotted in Fig. 24

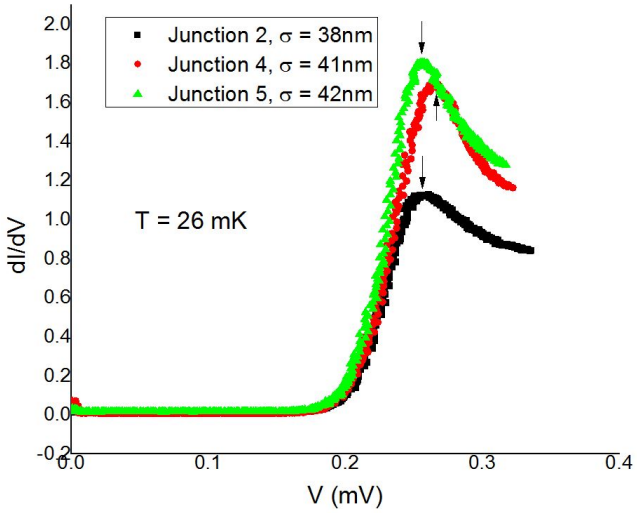

Figure 21: $\frac{dI}{dV}$-characteristics of SIS-junctions of sample 72. Peak marks the point of $\Delta_{Al} + \Delta_{Ti}$ feature of the junction (denoted by arrow). It should be noted that wire 2 did not exhibit a superconducting $R(T)$ transition, so it is possible that $\Delta_{Ti} = 0$ in that wire. Notice the broadening of the peak as σ is decreased.

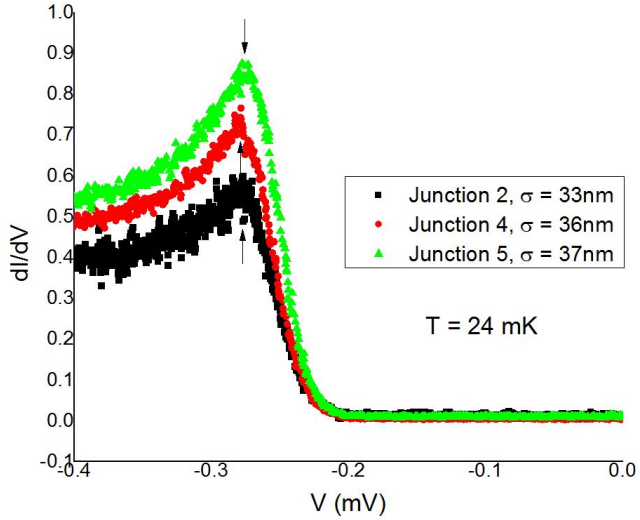

Figure 22: $\frac{dI}{dV}$-characteristics of SIS-junctions of the sample 72 after sputtering. Peak marks the point of $\Delta_{Al} + \Delta_{Ti}$ feature of the junction (denoted by arrow). Notice the broadening compared to Fig. 21 as diameter σ of the wires is decreased.

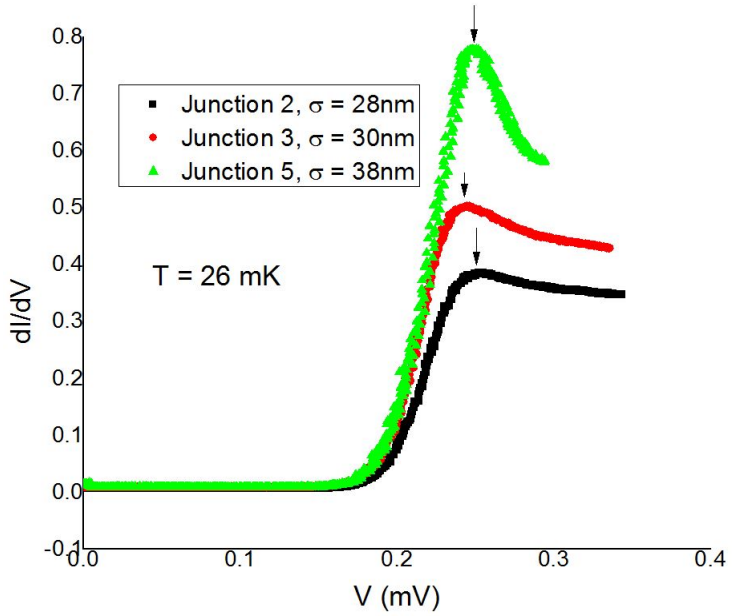

Figure 23: $\frac{\mathrm{d}I}{\mathrm{d}V}$-characteristics of SIS-junctions of the sample 74. Peak marks the point of $\Delta_{Al} + \Delta_{Ti}$ feature of the junction (denoted by arrow).

Same trends can be seen in sample 74 (Fig. 23). No visible change of the expectation value of the energy gap $\langle\Delta_{Ti}\rangle$is noticed when the diameter is reduced. These values of $\langle\Delta_{Ti}\rangle$ in different nanowires are plotted in Fig. 24.

Best fit $\langle\Delta_{Ti}\rangle$ values are unusually high, whereas Δ_{Al} are somehow smaller than the expected $\frac{\Delta_{Al}}{e} \approx 190\ \mu$V. It should be noted that if it is assumed that aluminum has a constant energy gap Δ_{Al} (as is done in this thesis), it will automatically imply that we have the finite energy gap for titanium $\langle\Delta_{Ti}\rangle$ in all wires despite the fact that $R(T)$-curves do not show pronounced resistance vs. temperature drop for the thinnest wires. This could possibly arise from high amount of QPS events which destroy the superconductivity rapidly in some parts of the wire, resulting in weak $R(T)$ dependence, but the energy gap is still finite. Fig. 24 does not show any clear relation between $\langle\Delta_{Ti}\rangle$ and

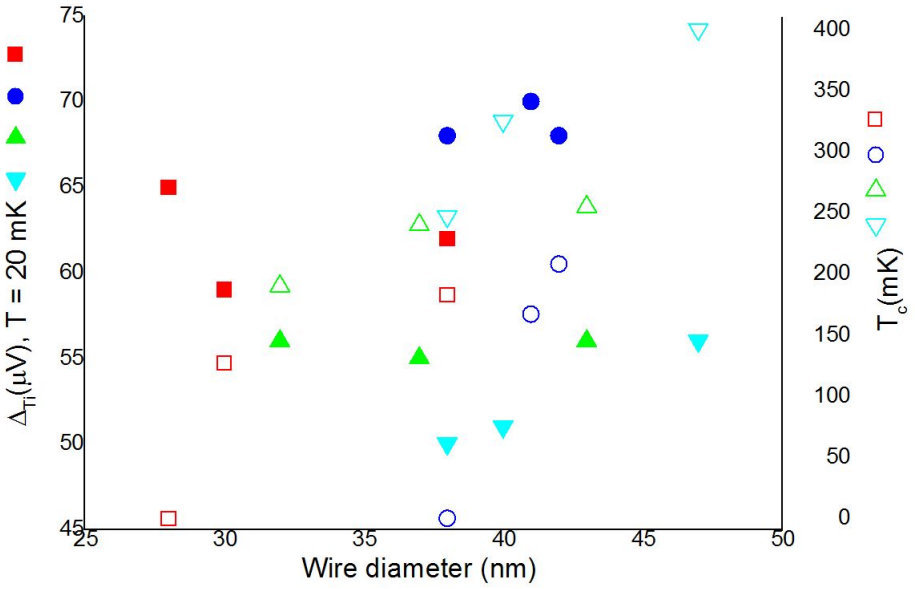

Figure 24: Values of the average energy gap $\langle \Delta_{Ti} \rangle$ (solid symbols, left axis) and the critical temperature T_c (open symbols, right axis) for four different nanowires with progressively reduced effective diameter (horizontal axis). Values of the average energy gap $\langle \Delta_{Ti} \rangle$ were obtained through measuring of the $I(V)$-dependencies of the tunnel SIS junctions, while the critical temperature T_c has been determined from $R(T)$ measurements of individual nanowires.

σ, but from differential conductance plots (Figs. 21 and 23) one can notice that broadening of Δ_{Ti} correlates with the nanowire diameter σ.

Another feature at $eV = |\Delta_{Al} - \Delta_{Ti}|$ is not clearly pronounced in thinnest wires. The observation is expected. Sharp feature at $eV = |\Delta_{Al} \pm \Delta_{Ti}|$ would be expected if in both materials the edge of the gap is very well defined. In practice, finite broadening of $|\Delta_1 \pm \Delta_2|$ features typically is accounted for, so called, Dynes broadening of the DOS (see next chapter) in both SC materials. In our case this, relatively small effect, is present. However, much stronger broadening originates from non-single-valued order parameter in titanium nanowires due to quantum fluctuations. This behaviour can also be seen from the simulations (next chapter).

4.4 Numerical analysis

From the $I(V)$-characteristics of an S_1IS_2-junctions values of the gap parameter $\Delta_{1,2}$ can be deduced. Starting point here is the thickest titanium wire with effective diameter $\sigma = \sqrt{d \cdot h} = \sqrt{51\text{ nm} \cdot 35\text{ nm}} \approx 42$ nm. Here, so called, bulk approximation is made, assuming that Δ_{Ti} and DOS of the titanium nanowire are almost the same as in bulk. DOS used in numerical calculations has a form

$$N_S = \left| \mathrm{Re}\left(\frac{\epsilon + i\Gamma}{(\epsilon + i\Gamma)^2 - \Delta^2} \right) \right| \tag{58}$$

which leads to tunnel current of an S_1IS_2 junction

$$I_{S_1IS_2} = \frac{G_{nn}}{e} \int_{-\infty}^{\infty} \mathrm{d}\epsilon \left[f(\epsilon) - f(\epsilon + eV) \right] \left| \Re\left(\frac{\epsilon + eV + i\Gamma_1}{\sqrt{(\epsilon + eV + i\Gamma_1)^2 - \Delta_1^2}} \right) \right| \cdot \left| \Re\left(\frac{\epsilon + i\Gamma_2}{\sqrt{\epsilon^2 + i\Gamma_2 - \Delta_2^2}} \right) \right| \tag{59}$$

where Γ_i is a so called Dynes parameter, not to be confused with the attempt rate mentioned in the theory. Parameter Γ characterises the smearing of the DOS. Finite values of Γ are typically associated with finite quasiparticle lifetimes. Clearly this reduces to formula (53) if $\Gamma_1 = \Gamma_2 = 0$. Using previous own experimental data we start from $\frac{\Gamma_i}{\Delta_i} \approx 0.01 \quad i = 1,2$. From the best fit, the final value of $\frac{\Gamma_{Al}}{\Delta_{Al}} = 0.04$ were chosen for the further calculations. For the rest of samples Δ_{Al} and Γ_{Al} were kept as constants. Example simulations are shown in Figs. 25 and 26

Now that other parameters are fixed, we can concentrate on Δ_{Ti} which is the subject of this study. The simulations are compared to measured data to find best possible fits for the parameter Δ_{Ti}. As noticed before, value of Δ_{Ti} varies so it should be taken into account when simulating the 'spread' of the value of the energy gap $\Delta_{Ti} = \langle \Delta_{Ti} \rangle \pm \delta\Delta_{Ti}$. For thicker nanowires fluctuations are expected to be small or even negligible. Smaller the diameter, higher the fluctuations and thus the smearing of the energy gap. Fig. 28 demonstrates how simulated $I(V)$ at $eV \approx |\Delta_{Al} - \Delta_{Ti}|$ smears out as the fluctuations of Δ_{Ti} increase. Simulations with different temperature T were also done, see Fig. 27

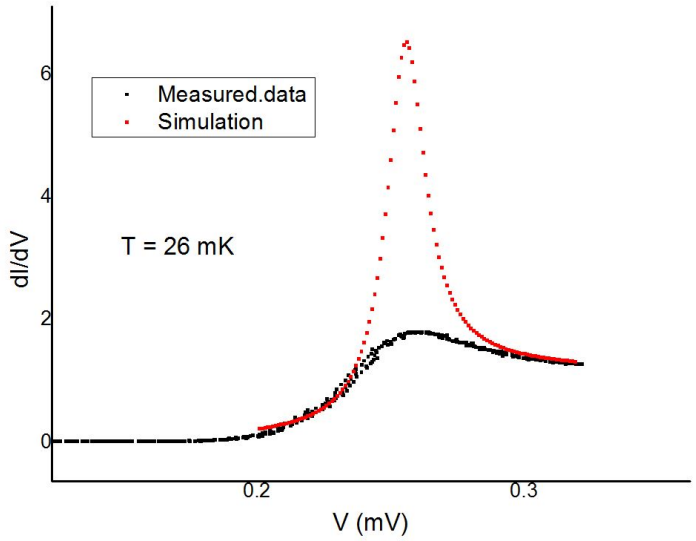

Figure 25: Theoretical fits and experimental $\frac{\mathrm{d}I}{\mathrm{d}V}$-characteristics for sample 72, junction 5. Simulation calculated with formula 59. Parameters used: $\frac{\Gamma_{Al}}{\Delta_{Al}} = 0.04$, $\frac{\Gamma_{Ti}}{\Delta_{Ti}} = 0.01$ with constant value of $\frac{\Delta_{Ti}}{e} = 55\ \mu$V.

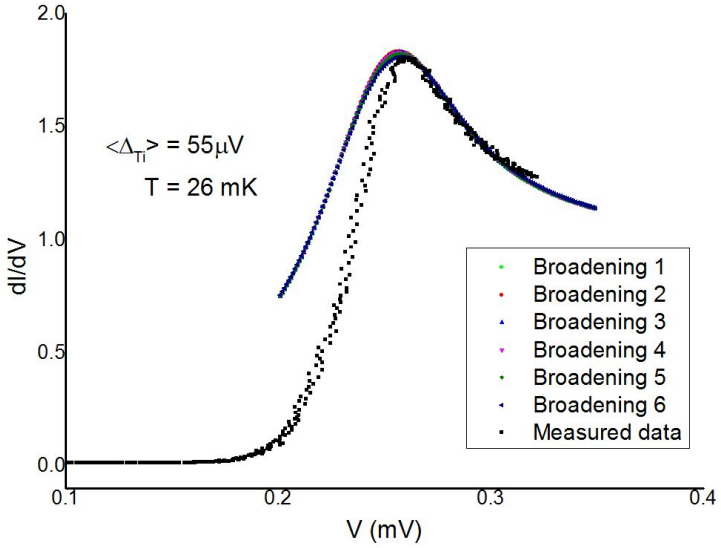

Figure 26: Theoretical fits and experimental $\frac{\mathrm{d}I}{\mathrm{d}V}$-characteristics for sample 72, junction 5. Distribution of Δ_{Ti} centered around $55\mu V$. For $\delta\Delta_{Ti}$ we used Gaussian distribution shown in Fig. 29. Here $\frac{\Gamma_{Al}}{\Delta_{Al}} = 0.2$, $\frac{\Gamma_{Ti}}{\langle\Delta_{Ti}\rangle} = 0.01$

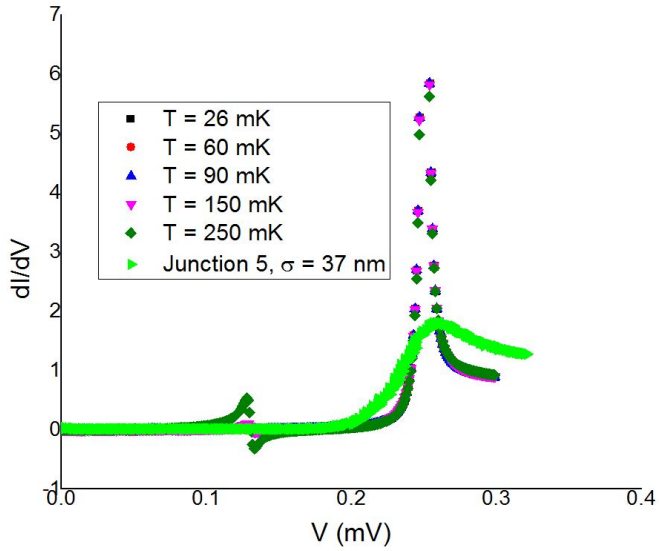

Figure 27: Theoretical fits in different temperatures T and experimental $\frac{\mathrm{d}I}{\mathrm{d}V}$-characteristics for sample 72, junction 5.

Similar smearing can be observed at $eV = |\Delta_{Al} - \Delta_{Ti}|$ peak. However, this feature is much less dependent on wire diameter σ. Similar Gaussian distributions (see Fig.29) were used here to obtain best possible correspondence with the data. Difference between the fits using the least and the most broadened energy gap is small at $eV = |\Delta_{Al} - \Delta_{Ti}|$ compared to the $eV = |\Delta_{Al} + \Delta_{Ti}|$ feature, but definitely visible. Larger broadening of energy gap has better correspondence with measured data.

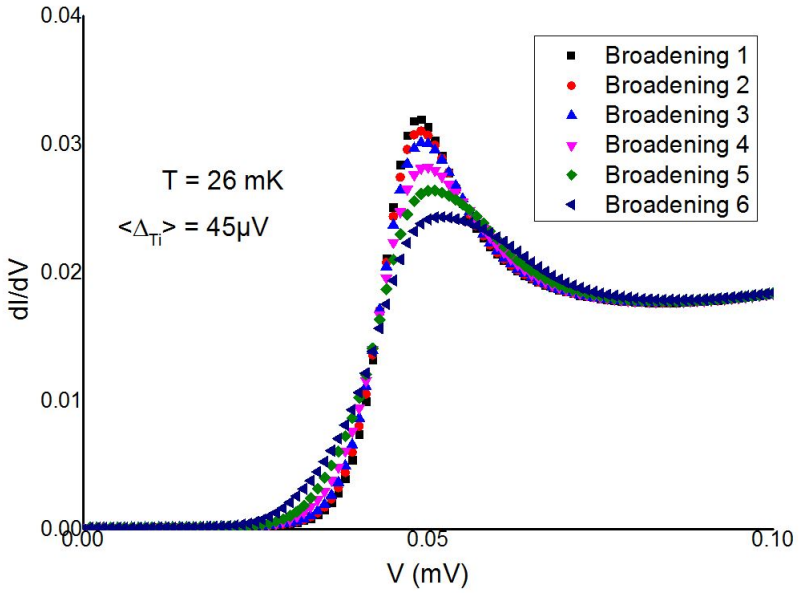

Figure 28: Simulated $I(V)$ dependence assuming distribution of $\frac{\Delta_{Ti}}{e}$ centered around 45 μV. Used Gaussian distributions are shown in Fig. 29

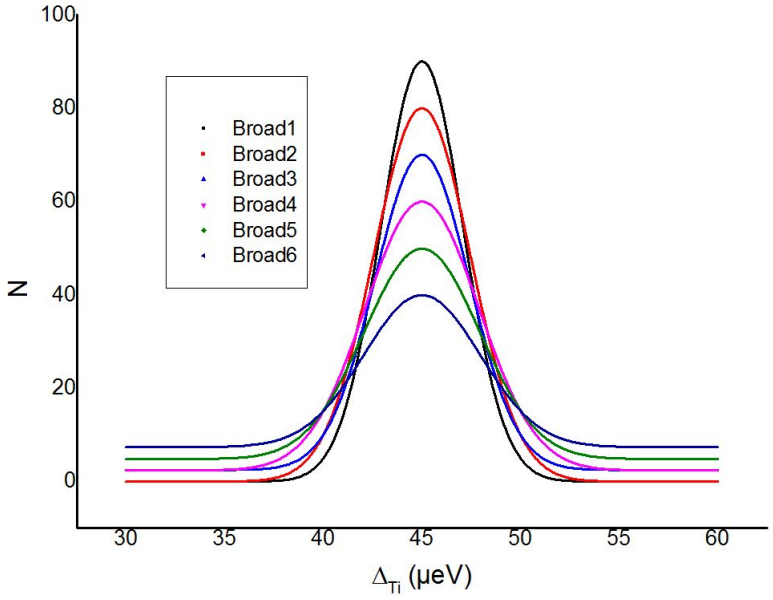

Figure 29: Model distributions of Δ_{Ti} in a nanowire. Distributions are centered around $\frac{\langle\Delta_{Ti}\rangle}{e} = 45$ μV.

4.5 Summary

Goal of this thesis is to study the impact of quantum fluctuations of the energy gap Δ in titanium nanowires. This phenomenon is assumed to rise from quantum fluctuations, also contributing to fluctuations of the phase of the complex order parameter $\Delta = |\Delta|e^{i\varphi}$. Three different samples with multiple titanium nanowires were studied. $R(T)$-, $I(V)$- and $\frac{\mathrm{d}I}{\mathrm{d}V}$-data were measured for all nanowires and S_1IS_2-junctions. Two of the samples, 72 and 74, have three measurable nanowires each and in both samples the thinnest wire does not exhibit $R(T)$ superconducting transition. Superconducting wires do show correlation between diameter of the wire σ and critical temperature T_c. Lack of pronounced $R(T)$ transition in thinnest wires is related to quantum phase slips (QPS), which destroy the superconductivity in one dimensional channels. QPS effect on transition was studied and results can be seen in Figs. 11 and 12. Good correspondence was obtained especially on the thicker wires where the applicability of the model [7] is mostly valid. In sample 82 there is a few nanometer layer of palladium deposited on top of aluminum oxide (under titanium). In this sample nanowires do not exhibit superconducting transition, but wider parts of the structure do.

$I(V)$-dependencies were measured and from those the value of the energy gap Δ_{Ti} was deduced. Results show that in quasi-one dimensional titanium nanowires the value of Δ_{Ti} is not longer a constant, but it's value has a statistical distribution which is a consequence of QFs. This has several impacts on $I(V)$-characteristics of an S_1IS_2-junction: the feature around point $|\Delta_{Al} \pm \Delta_{Ti}|$ is not a sharp peak anymore, but it broadens due to smearing of the DOS edge. Because of this, the feature can disappear almost completely in the thinnest wires (Fig. 20). Another possibility is that Dynes parameter Γ also varies as a function of σ, but that has not been studied in this thesis. The origin of the Dynes parameter is the finite quasiparticle lifetime, we assumed that this effect should be not size-dependent, unless the smallest dimension of the sample starts to be comparable with the grain size: $\sim$ 2 nm in titanium films and nanowires studied in this work. Mean values of $\langle\Delta_{Ti}\rangle$ were significantly different from what was expected: typically in titanium nanostructures $\langle\Delta_{Ti}\rangle =$

$(50-70)\mu eV$, but in our samples the best-fit values here are around 45 μV, as seen in Figs. 26,28 and 29. In earlier measurements values of $\langle\Delta_{Ti}\rangle$ were with in the expected range (Fig. 30). Reason for the difference is not known, and further study is needed for that.

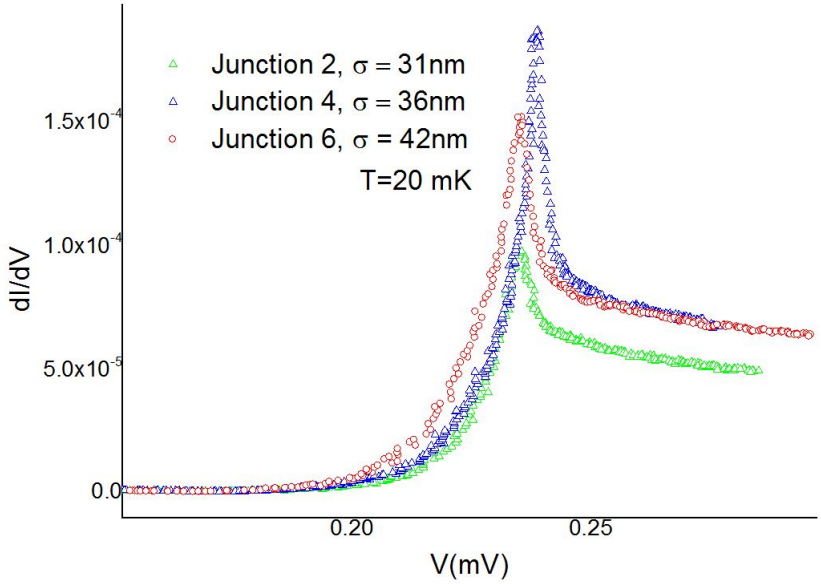

Figure 30: $\frac{\mathrm{d}I}{\mathrm{d}V}$-characteristics of SIS-junctions of the sample 31.

Simulations were done by using formula (59) to interpret the effects of spreading of the energy gap of titanium $\Delta_{Ti} = \langle\Delta_{Ti}\rangle \pm \delta\Delta_{Ti}$. Thickest wire was selected first to fix other parameters than Δ_{Ti}. After that Δ_{Ti} was varied through large energy range and statistical distributions to simulate quantum fluctuations of the energy gap. Simulations show that QFs can smear out the characteristic feature of S_1IS_2-junction, the sharp rise of current $I_{S_1IS_2}$ at $eV = |\Delta_{Al} + \Delta_{Ti}|$. Fluctuations cause the free energy states at $eV = |\Delta_{Al} - \Delta_{Ti}|$ to spread to a wide energy range (as Δ_{Ti} is no longer a constant), thus giving small current at that energy range. This is demonstrated in Fig. 28. Good quantitative correspondence with measured data and simulations was not obtained. Qualitatively it can be stated that a statistically distributed Δ_{Ti} gives better results than the single valued Δ_{Ti}. Simulated peak at $eV = |\Delta_{Al} + \Delta_{Ti}|$ has too

high values compared to the experiment. More study is needed for this. Presumably size-dependent variation of the Dynes parameter Γ_{Ti} should be also taken into consideration.

5 Publications

- T. Rantala, K. Yu. Arutyunov "Quantum Fluctuations of the superconducting energy gap in 1D superconductors", poster at Physics Days - 2012, Helsinki, March 2012.

- T. Rantala, J. S. Lehtinen, K. Yu. Arutyunov, "Quantum Fluctuations of the superconducting energy gap in 1D superconductors", poster at the Eighth International Conference in School format on Vortex Matter in Nanostructured Supercondcutors VORTEX-III, Rhodes-Greece, 21-26 September, 2013, abstract booklet p. 45.

- J. S. Lehtinen, T. Rantala, K. Yu. Arutyunov, "Quantum fluctuations in 1D supercondcutors: physics and applications", oral talk at the Eighth International Conference in School format on Vortex Matter in Nanostructured Supercondcutors VORTEX-III, Rhodes-Greece, 21-26 September, 2013, abstract booklet p. 169.
- T. Rantala, K. Yu. Arutyunov, "Quantum Fluctuations of the superconducting energy gap in 1D superconductors", poster at NanoScience days, 23-24October 2013.

- J. S. Lehtinen, T. Rantala and K. Yu. Arutyunov, Insulating State of a Quasi-1-Dimensional Superconductor, Submitted to PRL, October 2013

References

[1] Michael Tinkham. *Introduction to Superconductivity: Second edition*. Dover Books, 2004.

[2] V. L. Ginzburg and L. D. Landau. On the theory of superconductivity. *Zh. Eksperim. i. Teor. Fiz.*, 20:1064–1082, 1950.

[3] L. P. Gor'kov. Microscopic derivation of the ginzburg-landau equation in the theory of superconductivity. *Zh. Eksperim. i. Teor. Fiz.*, 9:1364–1367, 1959.

[4] A. M. Hriscu. *PhD Thesis: Theoretical proposals of quantum phase-slip devices*. Oct 2012.

[5] J. S. Langer and Vinay Ambegaokar. Intrinsic resistive transition in narrow superconducting channels. *Phys. Rev.*, 164:498–510, Dec 1967.

[6] D. E. McCumber and B. I. Halperin. Time scale of intrinsic resistive fluctuations in thin superconducting wires. *Phys. Rev. B*, 1:1054–1070, Feb 1970.

[7] K. Yu. Arutyunov, A. D. Zaikin, and Golubev D. S. Superconductivity in one dimension. *Physics Reports*, 464:1–70, Jul 2008.

[8] B. D. Josephson. Possible new effects in superconductive tunnelling. *Phys. Lett.*, 1:251–253, Jul 1962.

[9] B. D. Josephson. Supercurrents through barriers. *Adv. Phys.*, 14:419–451, 1965.

[10] J. S. Lehtinen, T. Sajavaara, K. Yu. Arutyunov, M. Yu. Presnjakov, and A. L. Vasiliev. Evidence of quantum phase slip effect in titanium nanowires. *Phys. Rev. B*, 85:094508, Mar 2012.

[11] J. S. Lehtinen and K. Yu. Arutyunov. The quantum phase slip phenomenon in superconducting nanowires with a low-ohmic environment. *Supercond. Sci. Technol.*, 25:124007, Nov 2012.

[12] J. Lehtinen. *MsC Thesis: Experimental study of quantum fluctuations in titanium nanowires in highly resistive environment*. Dec 2009.